UNITED NATIONS EDUCATIONAL, SCIENTIFIC AND CULTURAL ORGANIZATION
INTERNATIONAL ATOMIC ENERGY AGENCY
INTERNATIONAL CENTRE FOR THEORETICAL PHYSICS
I.C.T.P., P.O. BOX 586, 34100 TRIESTE, ITALY, CABLE: CENTRATOM TRIESTE

H4.SMR/1013-23

SCHOOL ON THE USE OF SYNCHROTRON RADIATION IN SCIENCE AND TECHNOLOGY:
"John Fuggle Memorial"

3 November - 5 December 1997

Miramare - Trieste, Italy

Reality: Tangent Errors and Thermal Loads

C. Lenardi
Commission of the European Union
Joint Research Centre
Ispra (Varese) Italy

Reality:
Tangent Errors and Thermal Loads

C. Lenardi

Commission of the European Union, Institute for Advanced Materials,
Joint Research Centre, I-21020 Ispra (Va), Italy
and
Politecnico di Milano, Italy

Fourth School on the Use of Synchrotron Radiation
in Science and Technology: "John Fuggle Memorial"
Trieste (It) 3 November - 5 December 1997
Miramare Trieste, Italy

Introduction

Third generation synchrotron radiation sources deliver VUV/X-ray beams of unprecedented quality and power. Can the beam features be conserved downstream to the experiments?

Conservation of emittance

The tolerable increase of emittance by the optics should be comparable to the stability specifications of the source parameters expected from the machine (e.g. ±10% source size and beam divergence).

a) *fundamental limits*

- optical aberrations

b) *technological limits*

- surface quality of mirrors/gratings
- quality of single crystals
- strain-free mechanical mounting
- stability of the optical element

Emittance

horizontal emittance.

$$\varepsilon_x = \sigma_x \sigma'_x \text{ (mm mrad)} .$$

vertical emittance.

$$\varepsilon_y = \sigma_y \sigma'_y \text{ (mm mrad)} .$$

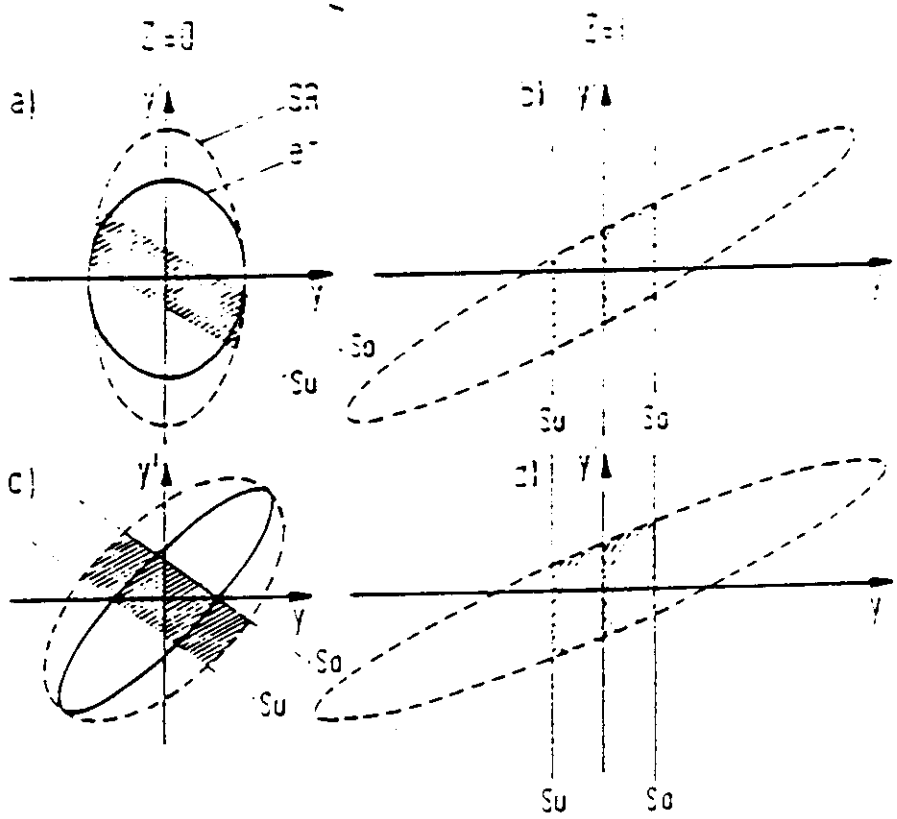

g. 22. Phase space ellipses for the vertical coordinate of the electron beam alone (solid lines) and luding the SR divergency (dashed lines). The source is located at $Z = 0$. the light beam expands in positive Z direction. The upright ellipse for SR at $Z = 0$ (a) is sheared while the beam moves to $= l$ (b). The invariants are the intersections with the y-axis. the projection on the y'-axis and the a. A slit (with boundaries S_u and S_o) inserted at $Z = l$ can be projected back to the origin (a). The ided area is an invariant also. Figures (c) and (d) show the same transformation for an already tilted ctron beam ellipse (divergent electron beam!). Similar graphs hold for the horizontal emittance (from Gudat and Kunz (1979)).

Synchrotron source characteristics

Brillance

$$n(x,z,\vartheta,\psi,\varepsilon,t)\ [\text{ph}\cdot\text{sec}^{-1}\cdot\text{mm}^{-2}\cdot\text{mrad}^{-2}\ per\ 0.1\%\Delta\varepsilon/\varepsilon]$$

n is the number of photons with energy ε emitted at a time t from a souce point (x,z) along the direction (ϑ,ψ) per time interval, unit source area, unit solid angle and 0.1% bandwidth.

Intensity

$$N(\vartheta,\psi,\varepsilon,t)=\int n\,dx\,dz\ [\text{ph}\cdot\text{sec}^{-1}\cdot\text{mrad}^{-2}\ per\ 0.1\%\Delta\varepsilon/\varepsilon]$$

N is given by integrating n over the source area.

Spectral flux

$$\phi_s(\varepsilon,t)=\int N\,d\vartheta\,d\psi\ [\text{ph}\cdot\text{sec}^{-1}\ per\ 0.1\%\Delta\varepsilon/\varepsilon]$$

ϕ_s is given by integrating N over the solid angle Ω.

Total flux

$$\phi_{tot}(t)=\int_0^\infty \frac{1}{\varepsilon}\phi_s\,d\varepsilon\ [\text{ph}\cdot\text{sec}^{-1}]$$

is given by integrating ϕ_s over the whole energy spectrum.

Surface quality

- Roughness
  Few Å rms (state-of-the-art: feasible!)

- Slope errors
  1÷2 μrad

Type of mirror	Standard	Special	Prospective
flat	0.5"	0.2"	0.02"
spheric	1÷2"	0.5"	
aspheric	4÷5"	1÷2"	0.5"

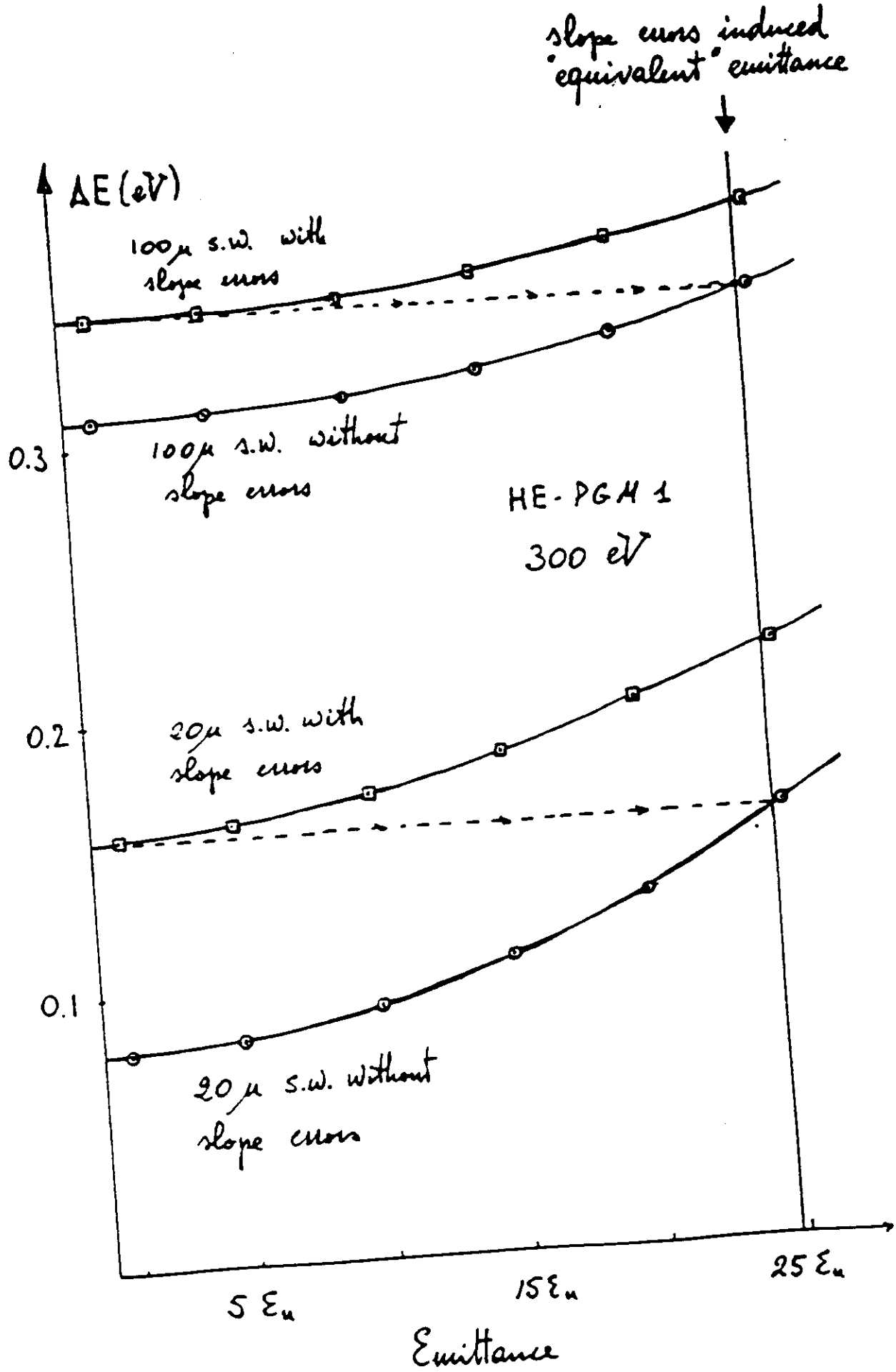
slope errors induced
"equivalent" emittance
ΔE (eV)
100 μ s.w. with
slope errors
100 μ s.w. without
slope errors
0.3
HE-PGM 1
300 eV
20 μ s.w. with
slope errors
0.2
20 μ s.w. without
slope errors
0.1
5 εu
15 εu
25 εu
Emittance

Conservation of brilliance

Thermally-induced slope errors and defective manufacturing of the optical elements yield a loss of brilliance, by far the acceptable tolerances. Thus a reduction of thermal distortions and figure errors are of fundamental relevance for preserving beam brilliance.

- The vertical source size is smaller than horizontal source size, thus for having high energy resolution the dispersive plane should be vertical, and thus the **vertical brilliance should be conserved**.

- In grazing incidence the influence of **sagittal** and **tangential errors** at the image plane are different.

Slope errors

- Reflection law:

$$\hat{r} = \hat{i} - 2(\hat{i} \cdot \hat{n})\hat{n}$$

$\hat{i}$ versor of the incident beam
$\hat{r}$ versor of the reflected beam
$\hat{n}$ versor of the normal to the surface

- Local variation of the normal $\delta\vec{n}$ implies a variation of the reflected beam:

$$\delta\vec{r} = -2\left[(\hat{i} \cdot \delta\vec{n})\hat{n} + (\hat{i} \cdot \hat{n})\delta\vec{n}\right]$$

- The deviation $|\delta\vec{r}_t|$ in the plane of incidence due to a variation $|\delta\vec{n}| = \delta\varphi$ is given by:

$$|\delta\vec{r}_t| = 2\sqrt{(\hat{i} \cdot \delta\vec{n})^2 + (\hat{i} \cdot \hat{n})^2 |\delta\vec{n}|^2} = 2\sqrt{\sin^2\alpha(\delta\varphi)^2 + \cos^2\alpha(\delta\varphi)^2} = 2\delta\varphi$$

- The deviation $|\delta\vec{r}_s|$ in a direction normal to the incidence plane due to a variation $|\delta\vec{n}| = \delta\varphi$ $(\hat{i} \cdot \delta\vec{n} = 0)$ is given by:

$$|\delta\vec{r}_s| = 2\sqrt{(\hat{i} \cdot \hat{n})^2 |\delta\vec{n}|^2} = 2\cos\alpha(\delta\varphi)$$

$|\delta\vec{r}_s|$ depends on the incident angle

- We suppose the distribution of slope errors to be gaussian: $\sigma = \delta\gamma$ (rms value). If the angular variation of the normal in tangential and sagittal planes are equal, it follows that $\delta\gamma = \sqrt{2}\,\delta\varphi$.

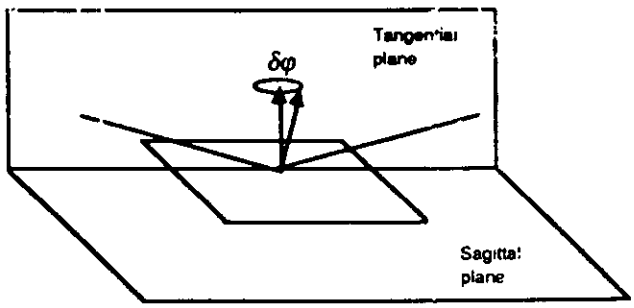

- aberration in the incidence plane:

$$\Delta z = 2 f \delta\varphi$$

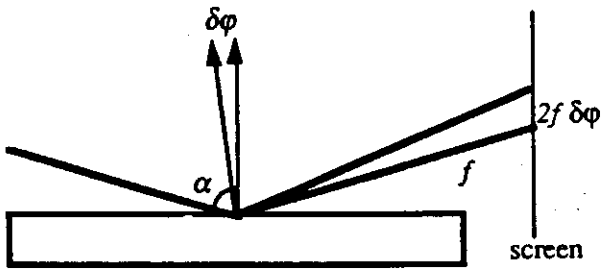

- aberration in a direction normal to the incidence plane:

$$\Delta y = 2 f \cos\alpha\, \delta\varphi$$

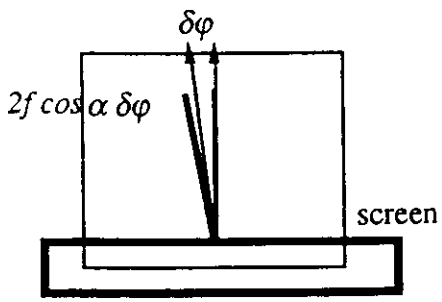

Example:

incident angle	α	= 87 deg
rms value of surface slope errors	$\delta\gamma$	= 1 arcsec (~ 5 μrad)
focal distance	f	= 3 m

$$\Delta z = 21.2\ \mu\text{m rms}$$

$$\Delta y = 1.11\ \mu\text{m rms}$$

Heat loading

- Third generation synchrotron radiation sources will deliver radiation beams with *unprecedented* ***power densities***. In particular multipolar magnetic devices, such as undulators and wigglers, will increase the brilliance of 4÷5 order of magnitude.

- Beamline performance depends critically on ***thermally-induced deformations*** (besides manufacturing slope errors).

Heat loading effects

- Degradation of the optical properties of beamline reflecting/diffracting components:

  - thermally induced deformations on optical surfaces produce focal image broadening and/or shift;

  - large amount of absorbed power upsets the designed optical figure.

- Radiation damage.

- Breaking of the optical element.

- Total detrimental effects:
  - **loss in photon flux**
  - **loss in energy resolution**

INSERTION DEVICES
TYPICAL STRUCTURE

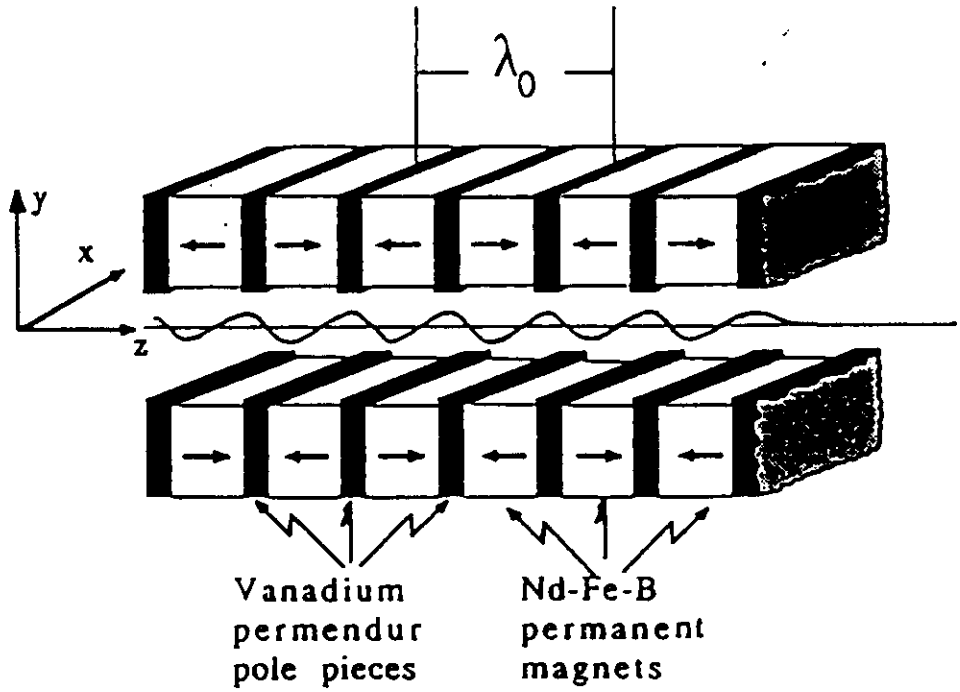

$$B = B_0 \cos(2\pi z/\lambda)$$

B_0(T) Peak Field at Poles

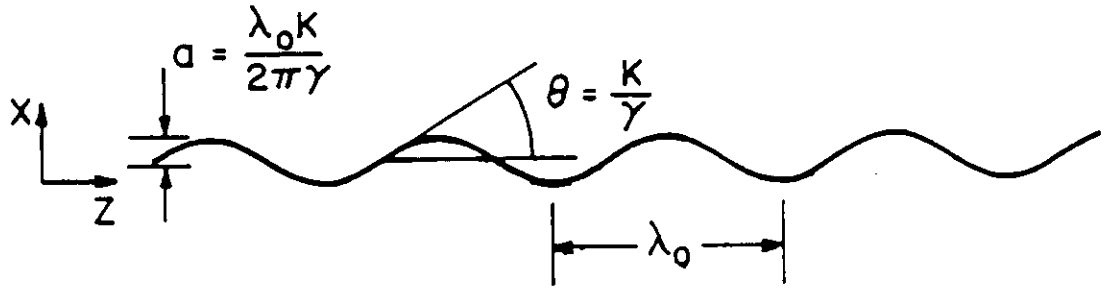

DEFLECTION PARAMETER $K = 0.934\,\lambda_0 B_0$

PARTICLE TRAJECTORY DETERMINES DEVICE CHARACTERISTICS

Total power for an ID source

$$P_{tot}\,[\mathrm{W}] = 1.263\, E_b^2 \langle B^2 \rangle I\, L$$

$$\langle B^2 \rangle \approx \frac{B_0^2}{2}$$

E_b storage ring energy [GeV]

B magnetic field [T]

I stored current [mA]

L ID length [m]

Angular distribution of power

(zero emittance)

$$\frac{d^2P}{d\theta\, d\psi}[\mathrm{W\cdot rad^{-2}}] = P_{tot}\frac{21\gamma^2}{16\pi K}G(K)\,f_K(\gamma\theta,\gamma\psi)$$

$$\frac{d^2P}{d\theta\, d\psi}[\mathrm{W\cdot mrad^{-2}}] = 10.84\,B_0\,E_b^4\,I\,N\,G(K)\,f_K(\gamma\theta,\gamma\psi)$$

θ horizontal observation angle

ψ vertical observation angle

N number of magnet periods

I stored current [A]

γ electron energy/m_ec^2

$\gamma = 1957\ E_b$ [GeV]

K deflection parameter

$K = 0.934\ \lambda_0$ [cm] B_0

$G\,(K)$ angle independent factor

$G(K) \rightarrow 1$ as K increases from 0

$f_K(\gamma\theta,\gamma\psi)$ normalized angular distribution function

$f_K(0,0) = 1$ (on-axis, peak power density)

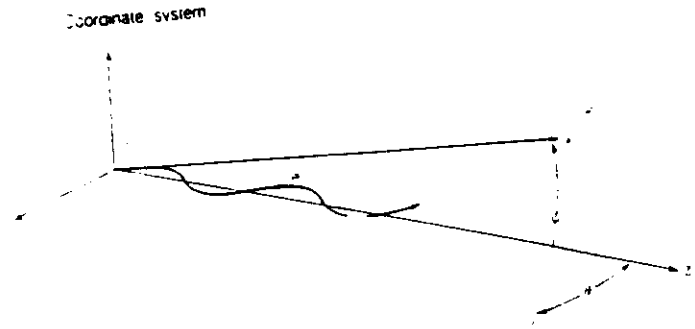

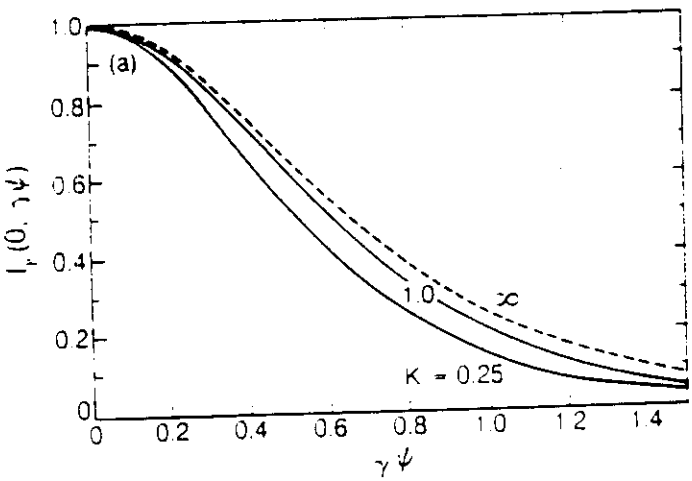

The behavior of the function $f_K(0, \gamma\psi)$.

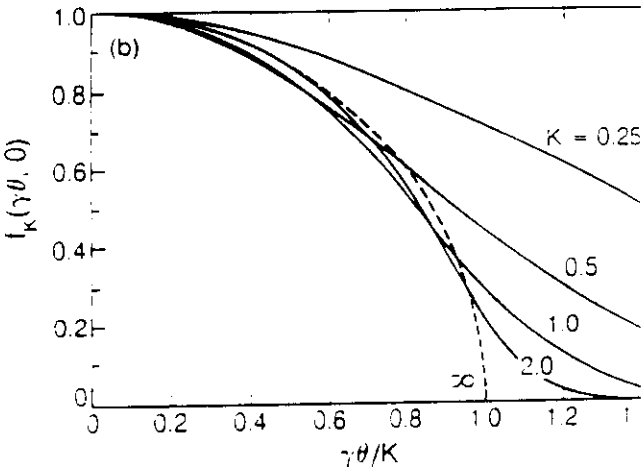

The behavior of the function $f_K(\gamma\theta, 0)$.

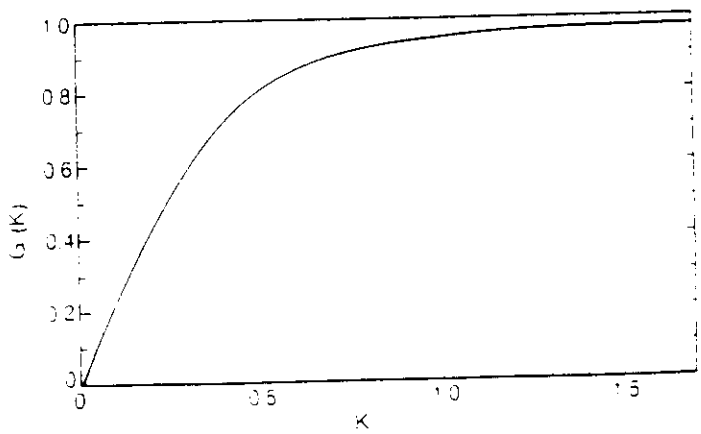

The behavior of the function $G(K)$.

Angular distribution function

The power envelope depends on the deflection parameter K.

Horizontal θ direction

$$\pm K / \gamma$$

Vertical ψ direction

$$\pm 1 / \gamma$$

If the ID works in the range of undulator mode ($K \leq 1$) the angular distribution of the nth harmonic is concentrated in a narrow cone whose half-width is given by:

$$\sigma_{\theta,\psi} \cong \sqrt{\frac{\lambda_n}{L}} = \frac{1}{\gamma}\sqrt{\frac{1+K^2/2}{2nN}}$$

n harmonic number

λ_n wavelength of nth harmonic

Power density per unit area

Normal incidence

$$\frac{d^2P}{dA}[\mathrm{W\cdot mm^{-2}}] = \frac{d^2P}{d\theta\, d\psi}[\mathrm{W\cdot rad^{-2}}]\ \frac{1}{R^2}[\mathrm{mm^{-2}}]$$

R distance from ID source

For a given impinging angle α

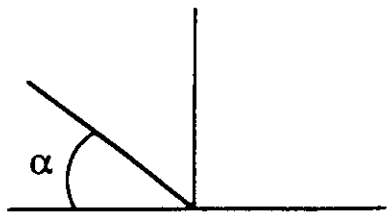

- Reduction of the power density by sin (α)

Footprint

- For normal incidence: half-widths of the spot

$$\sigma_x = \sigma_\theta R$$

$$\sigma_y = \sigma_\psi R$$

- For α impinging angle: an increment by 1/sin (α)

RELEVANT!

$$P_{tot} \sim E_b^2$$

$$\frac{d^2P}{d\theta d\psi} \sim E_b^4$$

TYPICAL ID PEAK POWER DENSITIES

	NSLS		SSRL		PEP	CHESS		APS		ALS	
	SUW x-ray	U5 vuv	VI	X	UND	WIG	UND	UND A	WIGA	U5	W13.6
B_0(T)	6	0.45	1.3	1.3	0.2	1.0	0.45	0.8	1.0	0.95	1.0
Poles	6	63	54	31	52	6	123	300	20	200	32
Length(m)	0.53	2.4	1.96	2.0	2.0	1.05	2.0	5.0	1.5	5.0	2.2
K	99	3	8	15	3	30	1.4	2.5	15	4	13
P_{total}(kW)	38	0.1	1.5	1.6	0.3	1.8	0.75	9.8	4.6	2.5	1.5
P(kW/mrad^2)	3.8	0.03	2.7	1.5	10	2.7	25	300	24	2.3	0.36
P(W/mm^2) @ 10 m	38	0.3	27	15	100	27	244	3000	240	23	3.6
σ'(v)mrad	0.12	0.4	0.1	0.1	0.04	0.06	0.06	0.044	0.044	0.2	0.2
σ'(h)mrad	20	2.	1.36	2.5	0.2	3	0.14	0.18	1.1	1.36	5.0

Angular Power Density

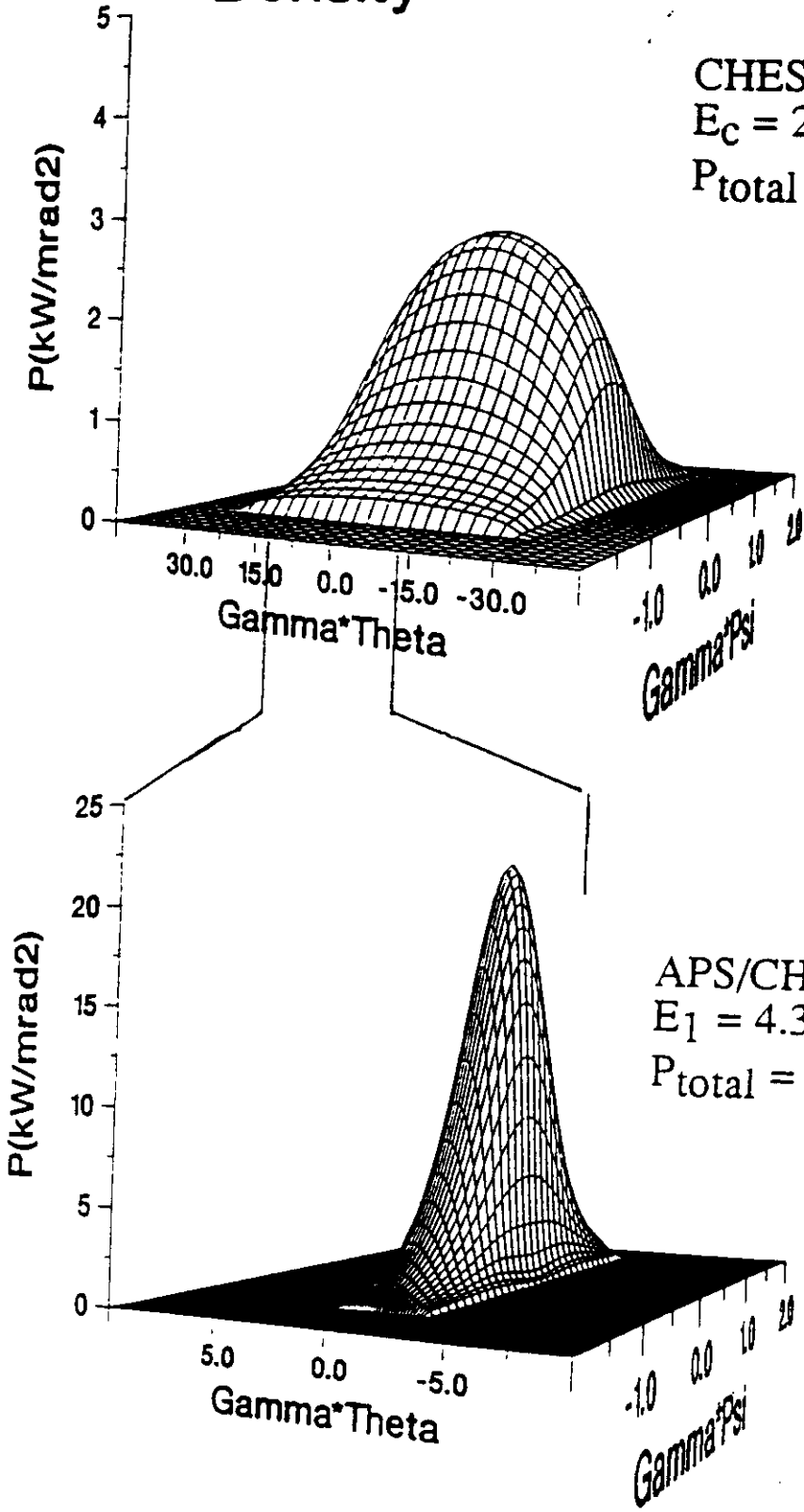

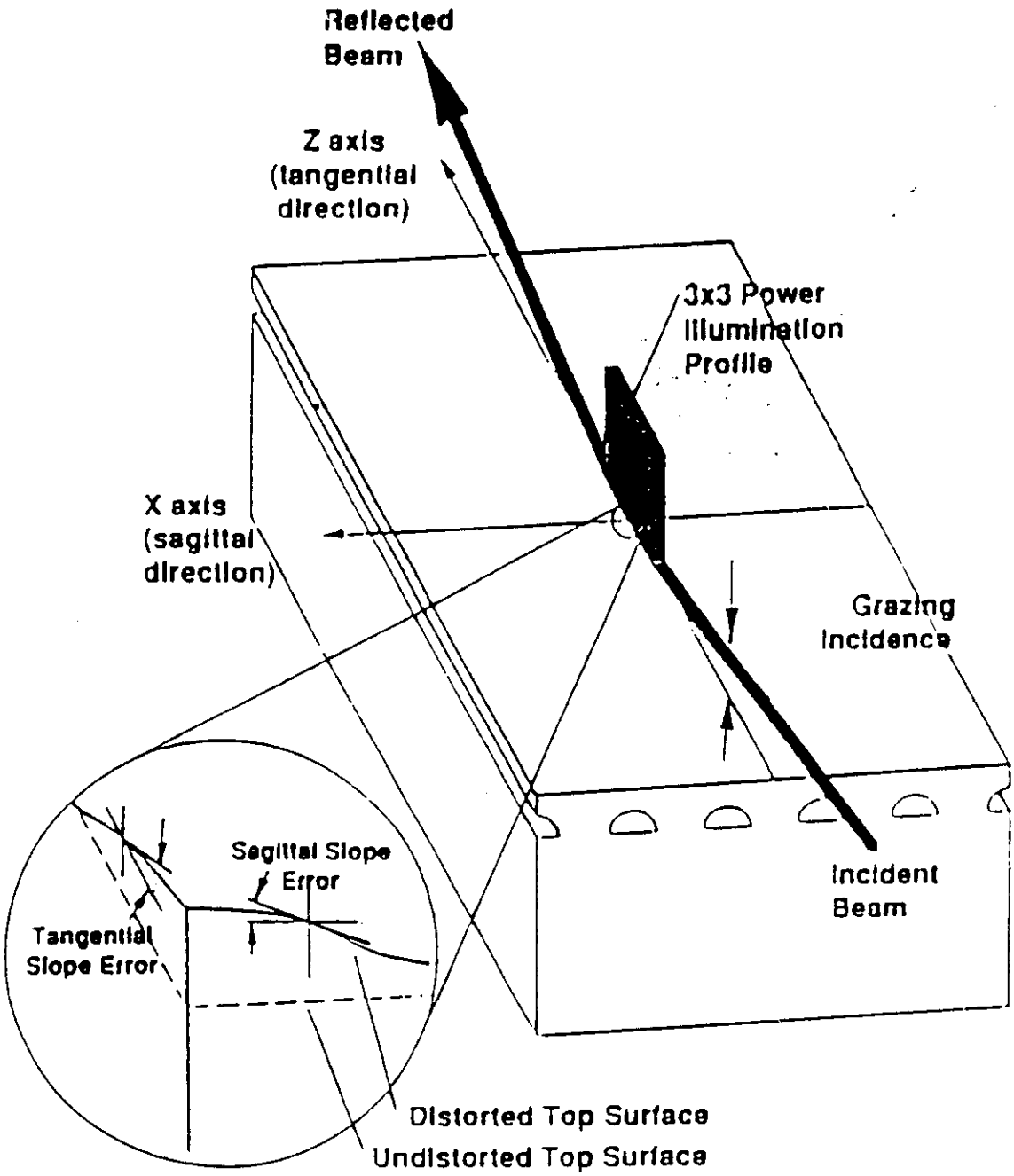
Reflected Beam
Z axis (tangential direction)
3x3 Power Illumination Profile
X axis (sagittal direction)
Grazing Incidence
Incident Beam
Sagittal Slope Error
Tangential Slope Error
Distorted Top Surface
Undistorted Top Surface

2 CRYSTAL MONOCHROMATOR

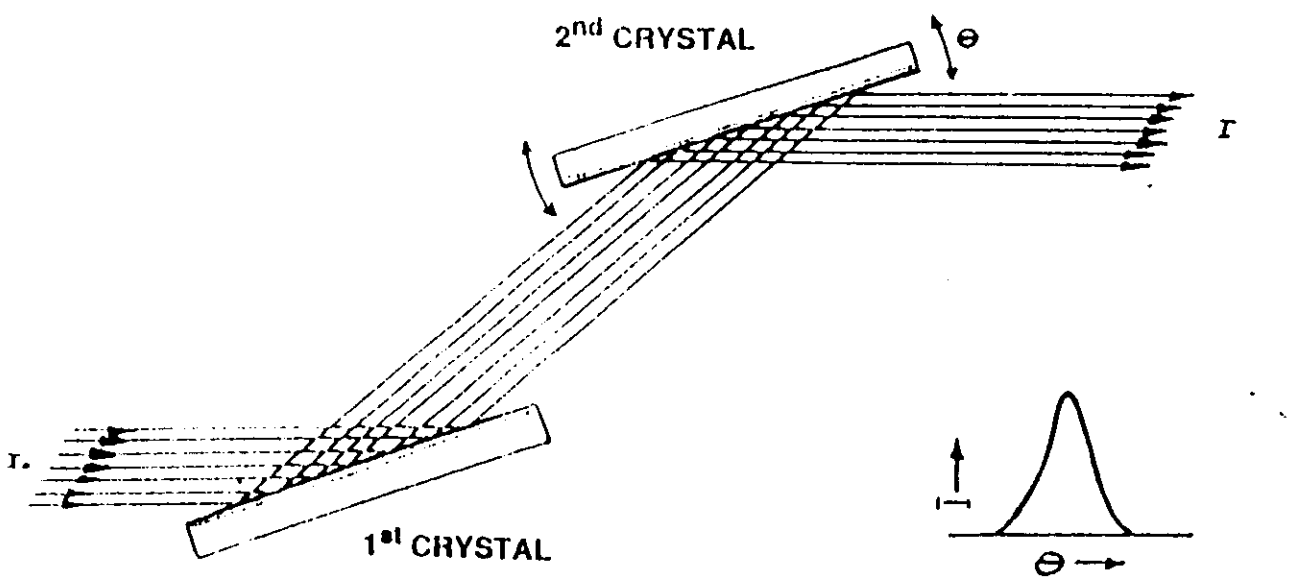

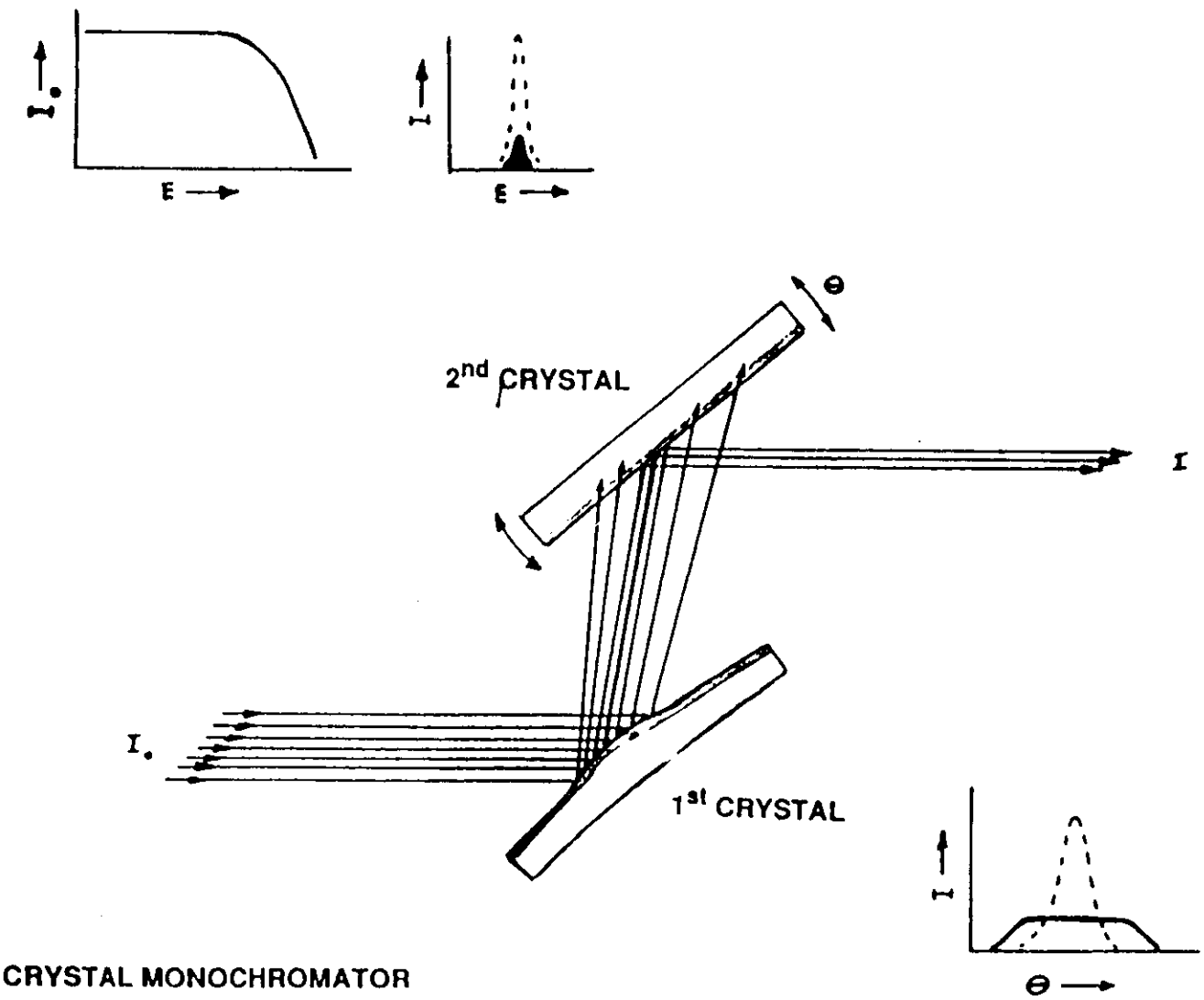

2 CRYSTAL MONOCHROMATOR

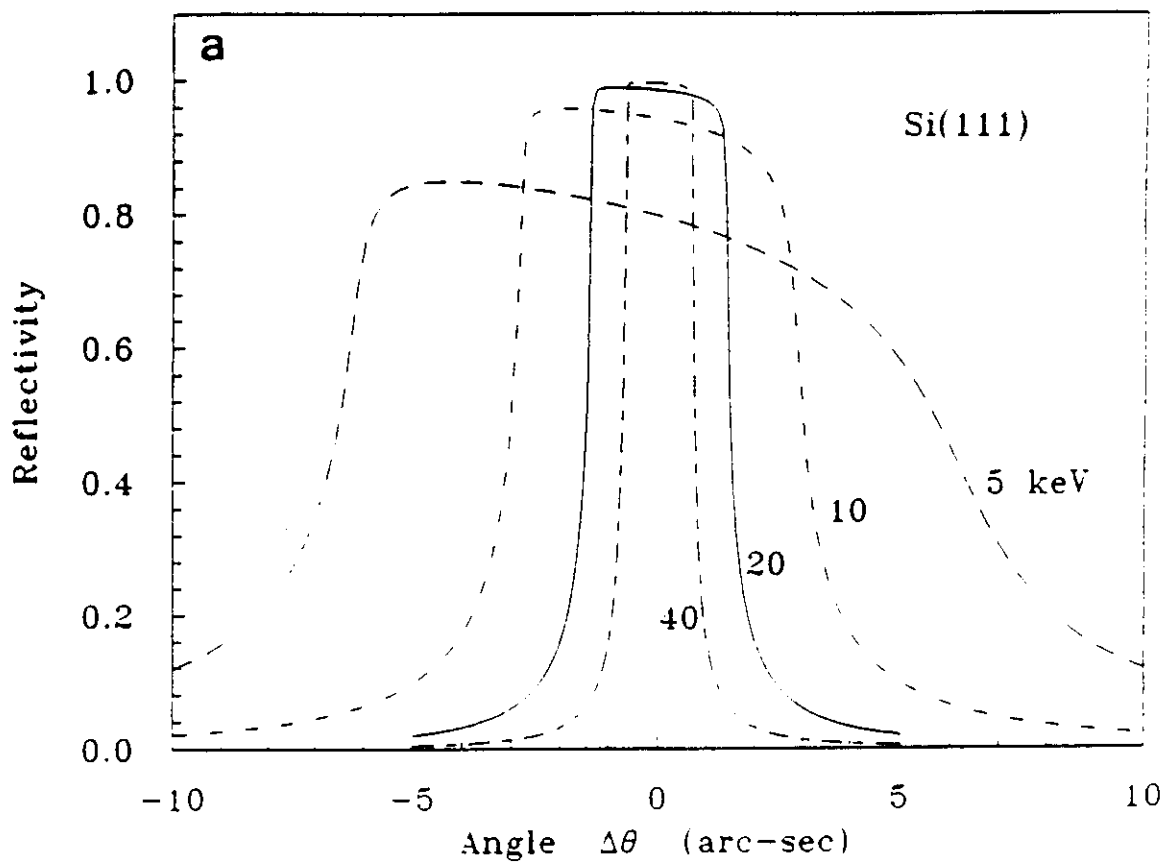
a
Si(111)
5 keV
10
20
40
Reflectivity
1.0
0.8
0.6
0.4
0.2
0.0
−10
−5
0
5
10
Angle Δθ (arc−sec)

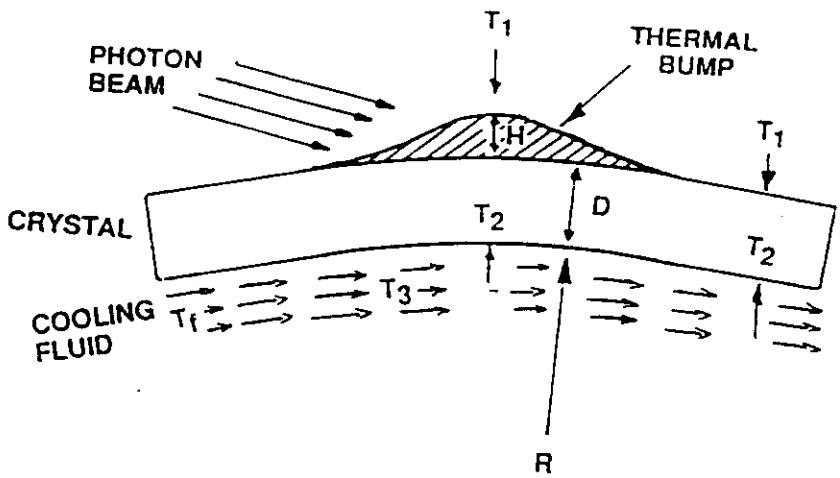

Schematic drawing of a silicon crystal showing distortion resulting from the high heat load of an intense x-ray synchrotron beam.

Thermal Distortions

Scheme:

a) the crystal is a plate of uniform thickness
b) no spreading of the heat parallel to the surface
c) backside cooling

- $T_1 = \Delta T_{12} + \Delta T_{23} + \Delta T_3 + T_f$
- $\Delta T_{12} = T_1 - T_2 = \frac{D\,Q}{k}$
- $\Delta T_{23} = T_2 - T_3 = \frac{Q}{h}$
- $\Delta T_3 = T_3 - T_f = \frac{1}{H_c V_a C_V} \int Q(x)\,dx$
- $\Delta T_1 = T_1 - T_f$

$-T_1$	temperature of the diffraction surface [°C]
$-T_2$	temperature of the crystal in contact with the fluid [°C]
$-T_3$	average temperature of the fluid [°C]
$-T_f$	bulk temperature of the fluid [°C]
$-D$	thickness of the crystal above the cooling channel [cm]
$-Q$	heat flux per unit area [$W \cdot cm^{-2}$]
$-k$	thermal conductivity of the crystal [$W \cdot cm^{-1} \cdot °C^{-1}$]
$-h$	film coefficient [$W \cdot cm^{-2} \cdot °C^{-1}$]
$-C_V$	volume specific heat of the fluid [$J \cdot cm^{-3}$]
$-H_c$	depth of the cooling channel [cm]
$-V_a$	average velocity of the fluid [$cm \cdot sec^{-1}$]

Three different components of distortion

1. bending

caused by the thermal expansion of the crystal in the direction parallel to the surface, due to the thermal variation along the depth of the crystal. The radius R of the bowing is:

$$R = \frac{D}{\alpha \Delta T_{12}} = \frac{k}{\alpha Q}$$

α [$^{\circ}C^{-1}$] thermal expansion coefficient.

Remarks:

- R is proportional to figure of merit k/α.
- R does not depend on crystal thickness D.
- R is independent on the cooling efficiency.
- The thickness of the crystal below the cooling channel stiffens the crystal and reduces the bowing.

Approximately the change in the angle of the surface is given by:

$$\Delta\Theta_s = \frac{\alpha}{k} Q \Delta L = \frac{\Delta L}{R}$$

ΔL distance along the bowed surface

Example:

Silicon Crystal:
$\alpha = 2.5\ 10^{-6}\ °C^{-1}$; $k = 1.5\ W \cdot cm^{-1} \cdot °C^{-1}$;

- heat flux $Q = 100\ W \cdot cm^{-2}$

$$R = 6\ 10^3\ cm$$

and the "bowing distortion" for unit length is:

$$\Delta\Theta_s = 34\ arcsec \cdot cm^{-1}$$

2. bump

caused by the thermal expansion of the crystal in the direction perpendicular to the surface, due to the thermal variation along directions parallel to crystal surface. The height H of the bump is given by:

$$H = \alpha D\left(\frac{\Delta T_{12}}{2} + \Delta T_{23} + \Delta T_3\right)$$

that is:

$$H = \alpha\left(\frac{QD^2}{2k} + \frac{QD}{h} + \Delta T_3 D\right)$$

Remarks:

- H is proportional to the expansion coefficient α.
- For large crystal thickness the first term dominates and H depends mostly on value of D.
- For small value of D the second term dominates and H is inversely proportional to h that is related with the cooling efficiency of the fluid.

- For reducing the bump:
  ===> **improvement of the figure of merit k/α.**
  ===> **thin crystals**
  ===> **high cooling efficiency**

Approximately the shape of the bump can be considered Gaussian, then the maximum slope error is given by:

$$\Delta\theta_{max} = \pm 1.4 \frac{H}{FWHM\,(spot\ size)}$$

FWHM depends on the spot size on the crystal

Example:

Silicon Crystal:

$\alpha = 2.5\ 10^{-6}\ °C^{-1}$; $k = 1.5\ W \cdot cm^{-1} \cdot °C^{-1}$; $D = 0.2$ cm; $H_c = .25$ cm.

- heat flux $Q = 100\ W \cdot cm^{-2}$; $FWHM = 2$ cm; $V_a = 100\ cm \cdot sec^{-1}$

- Liquid Gallium ($C_v = 2.4\ J \cdot cm^{-3}$)

  $\rightarrow$ $h = 5\ W \cdot cm^{-2} \cdot °C^{-1}$

  $\rightarrow$ $\Delta T_3 = 1.7\ °C$

$$H = 0.14\,\mu m, \quad \Delta\theta_{max} = \pm 2.0 \text{ arcsec}$$

- Water ($C_v = 4.1\ J \cdot cm^{-3}$)

  $\rightarrow$ $h = 1\ W \cdot cm^{-2} \cdot °C^{-1}$

  $\rightarrow$ $\Delta T_3 = 0.4\ °C$

$$H = 0.54\,\mu m, \quad \Delta\theta_{max} = \pm 7.8 \text{ arcsec}$$

3. variation of the crystal lattice spacing

caused by the thermal gradient along the crystal.
The variation in the diffraction angle is given by:

$$\Delta\vartheta = \vartheta\,\alpha\,\Delta T_1$$

that is:

$$\Delta\vartheta = \vartheta\,\alpha\left(\frac{DQ}{k} + \frac{Q}{h} + \frac{1}{H_c V_a C_V}\int Q(x)\,dx\right)$$

Remarks:

- The d-spacing variation deforms asymmetrically the rocking curve.
- The angular error $\Delta\vartheta$ depends on figure of merit k/α and on the photon energy, as well as on the cooling efficiency.

Example:

Silicon Crystal:

$\alpha = 2.5\ 10^{-6}\ °C^{-1}$; $k = 1.5\ W \cdot cm^{-1} \cdot °C^{-1}$; (1,1,1) planes

$D = 0.2$ cm; $H_c = 0.25$ cm

- heat flux $Q = 100\ W \cdot cm^{-2}$; $V_a = 100\ cm \cdot sec^{-1}$;
  ϑ (8 keV) = 14.3 deg

- Liquid Gallium ($C_v = 2.4\ J \cdot cm^{-3}$)
  - → $h = 5\ W \cdot cm^{-2} \cdot °C^{-1}$
  - → $\Delta T_3 = 1.7\ °C$
  - → $\Delta T_1 = 35\ °C$

$$\Delta\vartheta = \pm 4.6 \text{ arcsec}$$

- Water ($C_v = 4.1\ J \cdot cm^{-3}$)
  - → $h = 1\ W \cdot cm^{-2} \cdot °C^{-1}$
  - → $\Delta T_3 = 0.4\ °C$
  - → $\Delta T_1 = 114\ °C$

$$\Delta\vartheta = \pm 14.7 \text{ arcsec}$$

- This shifts are similar to the widths of the rocking curve of perfect silicon crystal at this energy and cause a mismatch between the first and the second crystal in a double crystal monochromator.

First optical element

- X-ray mirror

  - *working condition*:
    . total external reflection
  - *optical function*:
    . deflecting/focusing
    . filtering
  - *thermal load*:
    . low glancing angle ==> large spread-out
  - *required slope error or figure tolerance*:
    . 1÷2 μrad

- Perfect single crystal

  - *working condition*:
    . Bragg diffraction
  - *optical function*:
    . monochromatizing
  - *thermal load*:
    . smaller incident angles ==> higher power density
  - *allowable thermal distortion of the atomic planes*:
    . within Darwin widths

Minimising heat load problem

- Use of cooled filters:
  - Graphite, Kr gas, Al, Be...
- Improving cooling efficiency:
  - Optimization of cooling geometry
  - Choice of coolant (H_2O, Ga, N_2, Propane...)
- Choice of materials:
  - SiC, Diamond...
- Various innovative schemes:
  - Heating from the backside
  - Thin crystals
  - Cryogenic cooling
  - Applying an opposite mechanical momentum

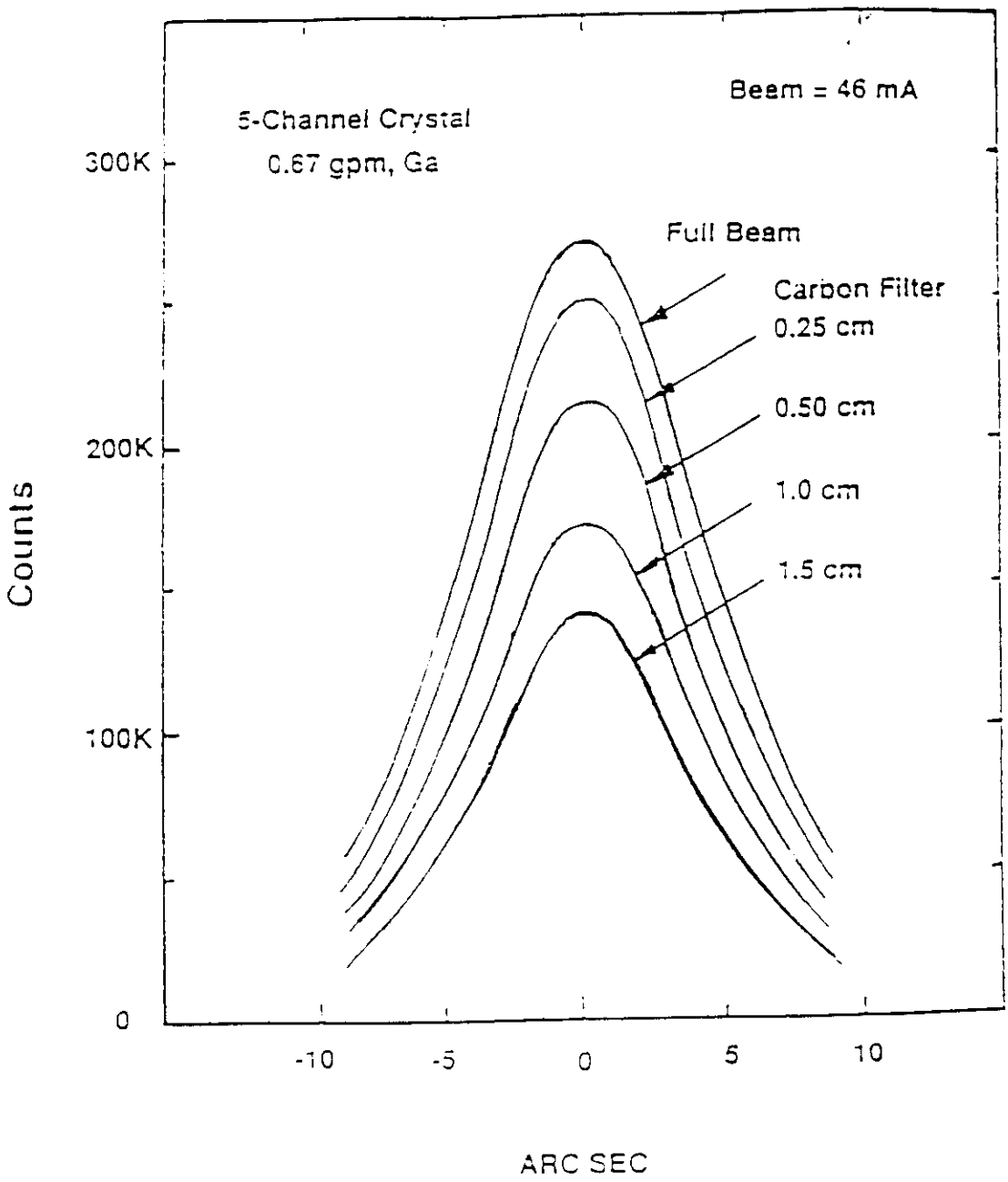

Plot of the counting rate from the diffracted beam of the CHESS two crystal monochromator as a function of the carbon absorber thickness in the beam.

Cooling geometries

a) **flat plate**:

. side and/or backside (i.e. water cooled copper block)

. efficient transfer medium (eutectic alloy InGa, In foil)

. for small heat loads (few W/cm^2)

. simple and more common solution

b) **channels**:

. increment of cooling efficiency

. increment of the effective transfer area

. thickness under the channels reduces the bowing

c) **microchannels**:

. features:

a) optimization of microchannel/fin widths

b) aspect ratio 10:1

c) increment of the cooled area by a factor of 10

d) laminar water flow

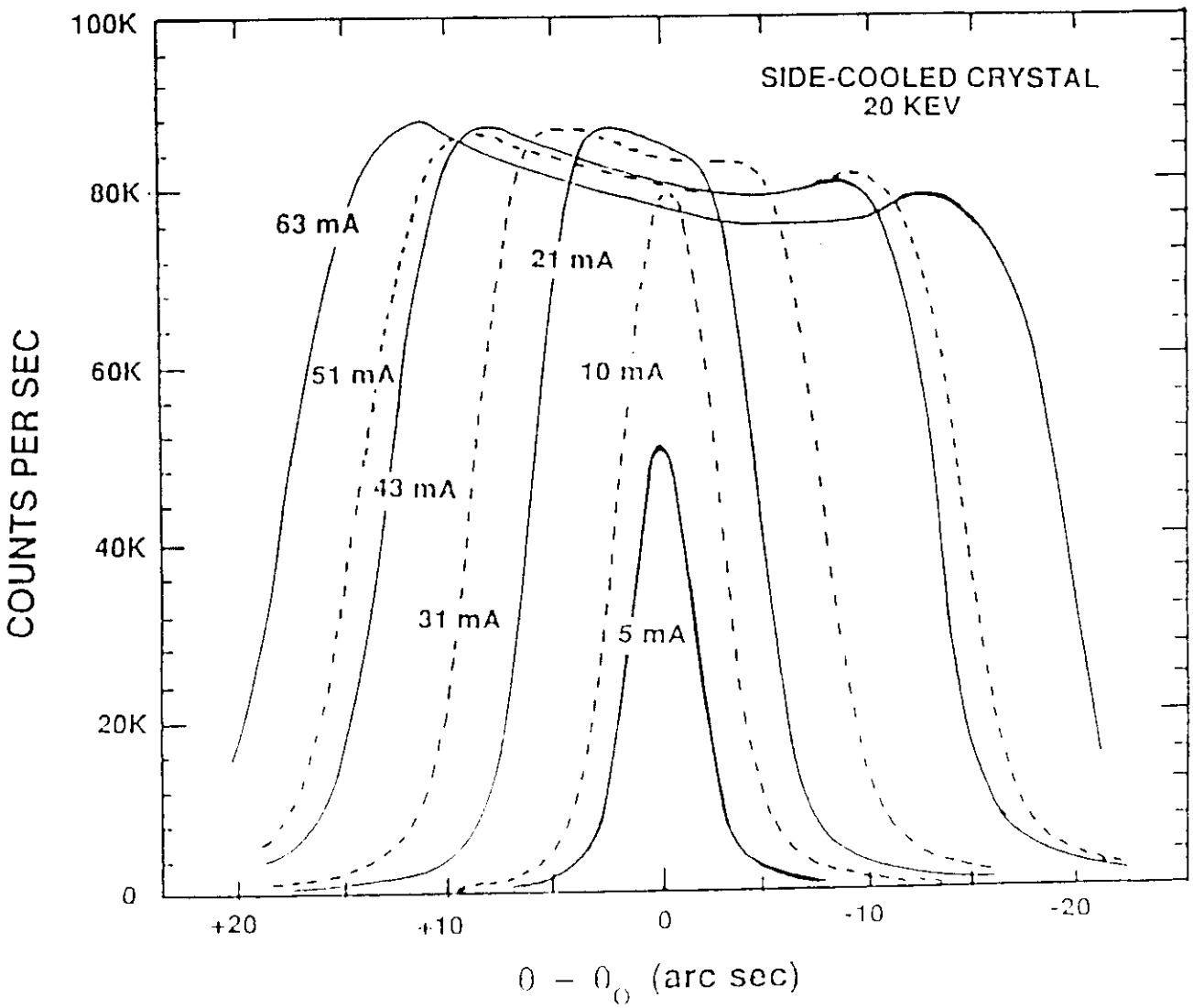

Rocking curves for the side-cooled, bottom-cooled crystal for different currents in the storage ring.

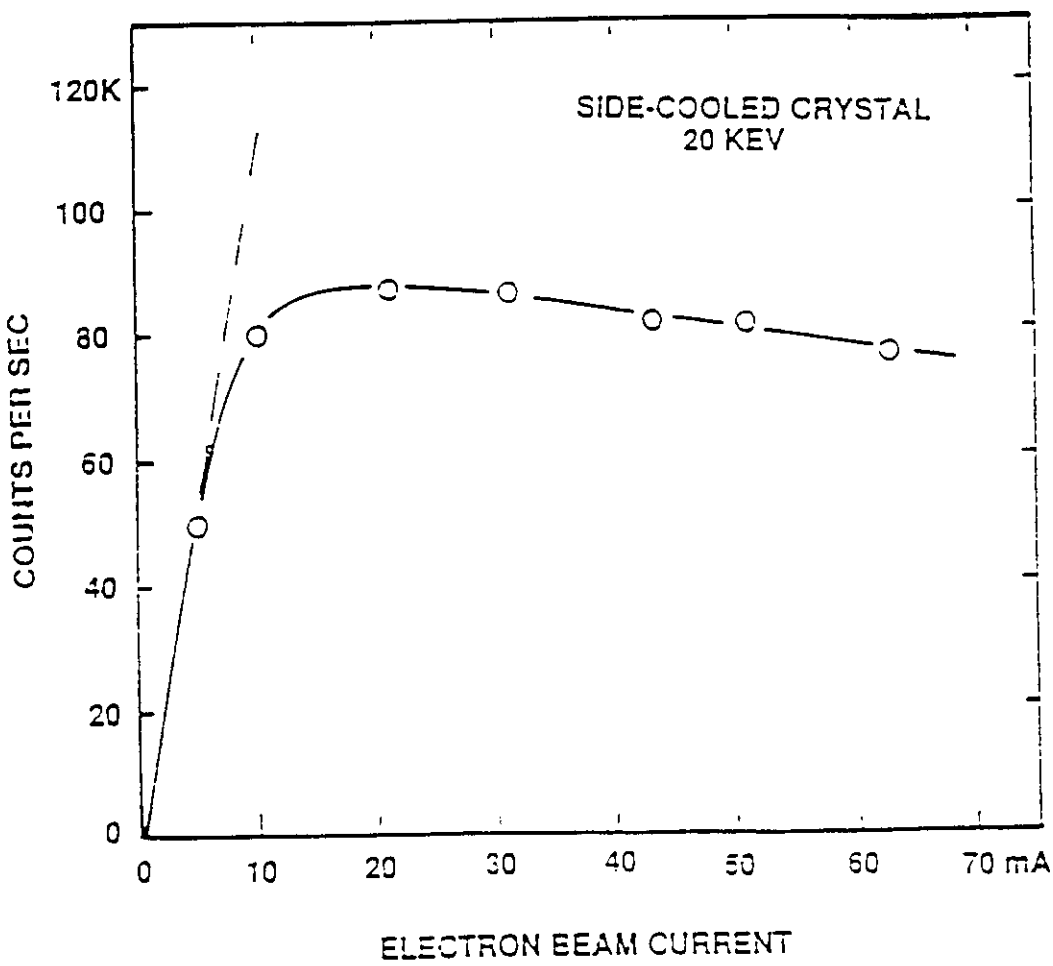

Plot of the peak counting rate in the CHESS two crystal monochromator versus electron beam current in the storage ring when the first crystal is the standard side-cooled, bottom cooled silicon (111) crystal.

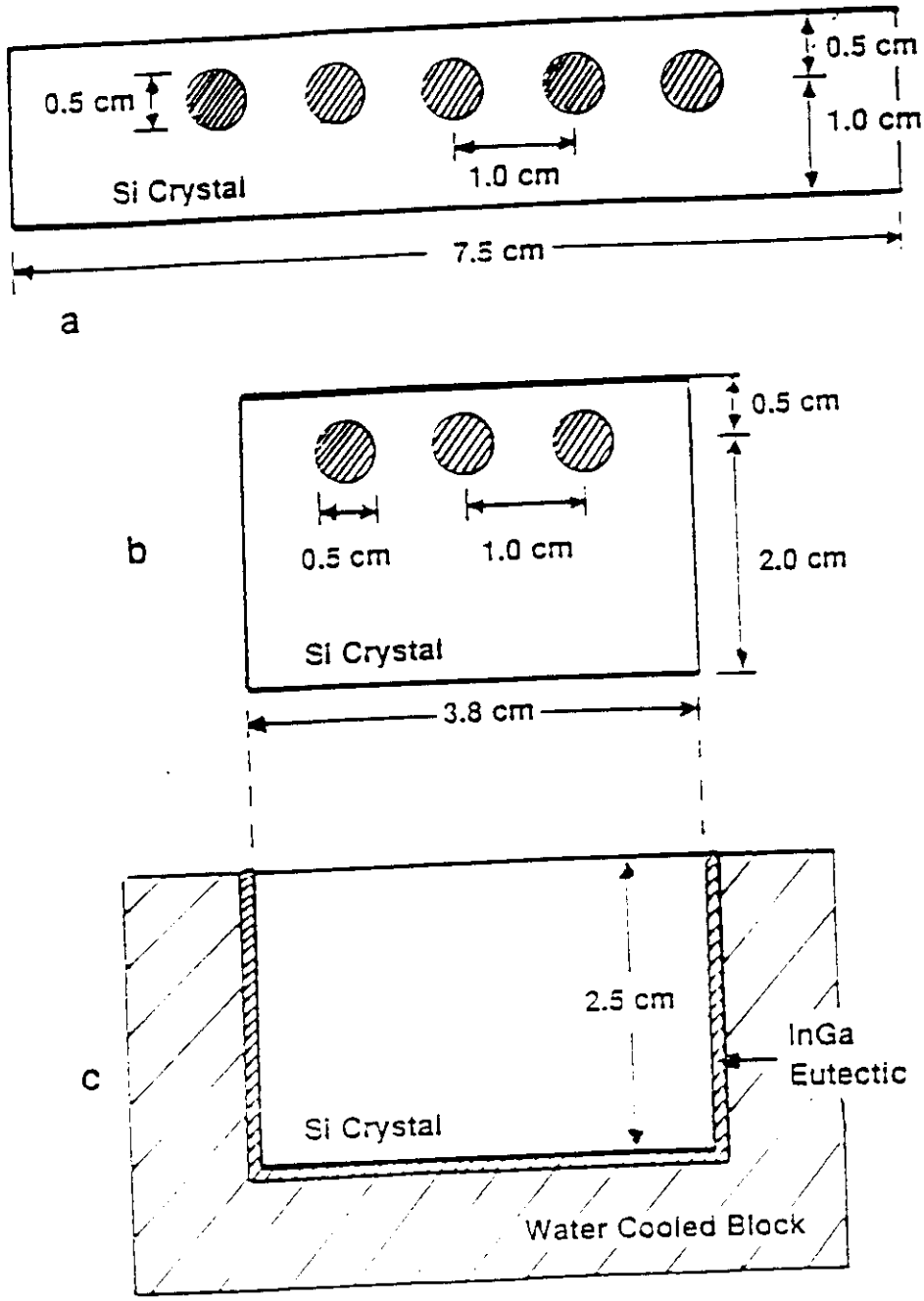

Drawings of the cross sections of the three cooled silicon crystals used in the wiggler experiments.

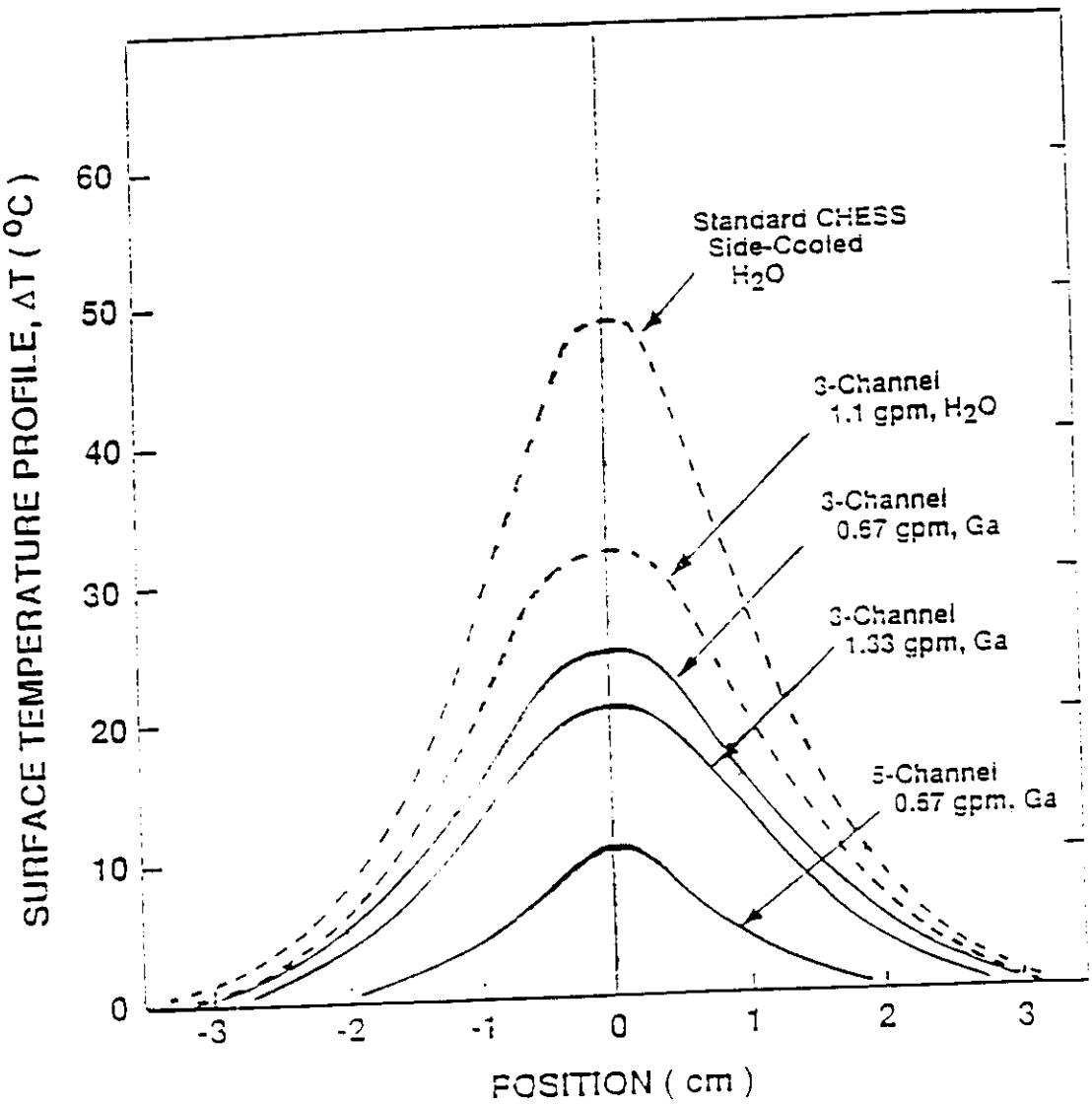

Plot of the surface temperature profile in the direction of the beam for the three different cooled silicon crystals used in the wiggler experiments.

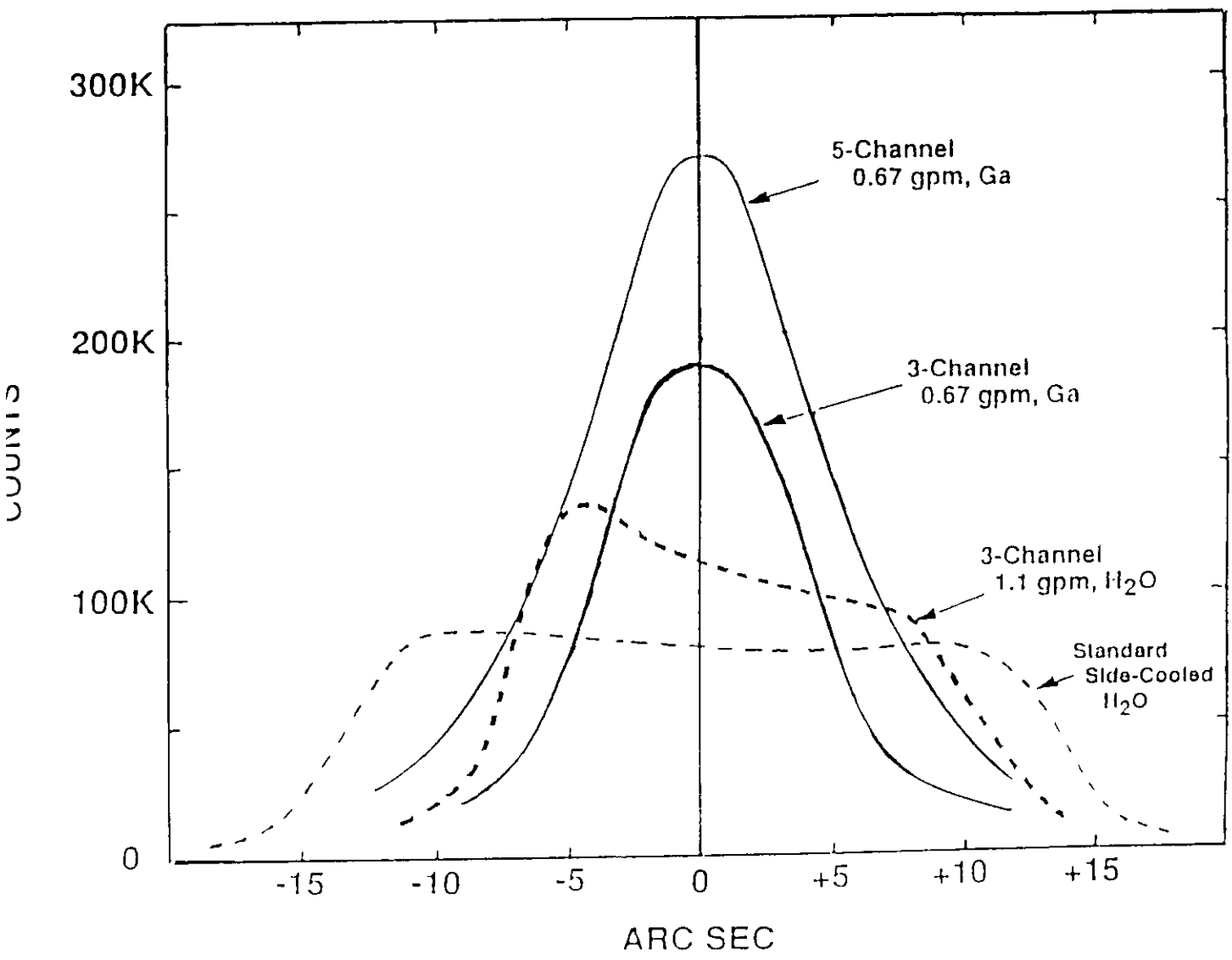

Plot of the rocking curves obtained with the three different silicon crystals in the wiggler experiments (photon energy = 20 keV, electron current = 46 mA).

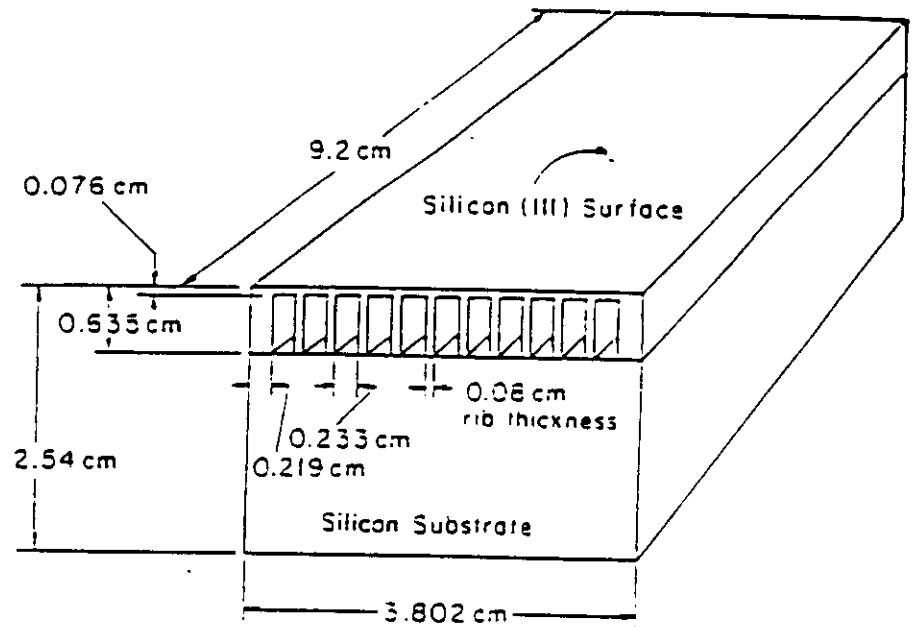
9.2 cm
0.076 cm
Silicon (111) Surface
0.635 cm
0.08 cm
rib thickness
0.233 cm
0.219 cm
2.54 cm
Silicon Substrate
3.802 cm

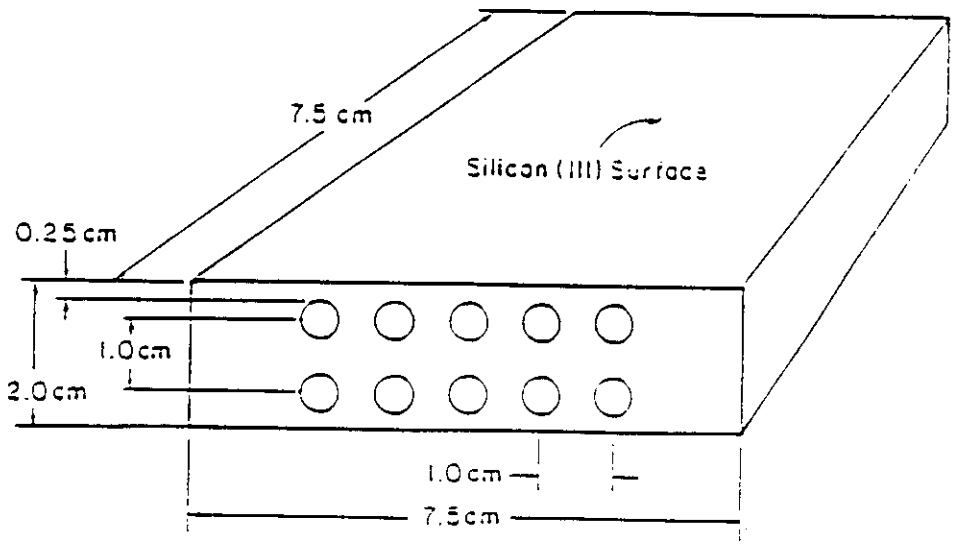
7.5 cm
Silicon (111) Surface
0.25 cm
1.0 cm
2.0 cm
1.0 cm
7.5 cm

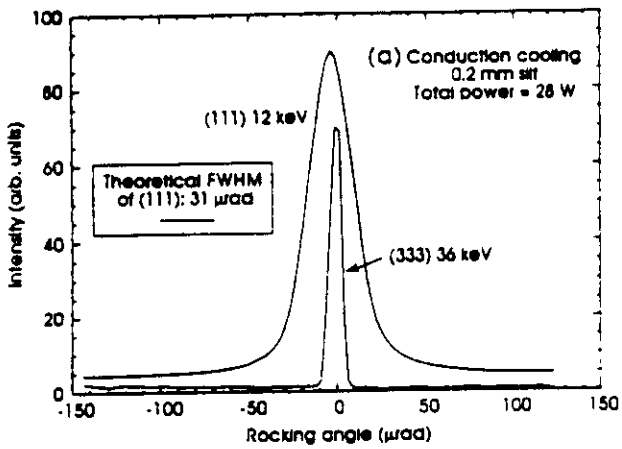

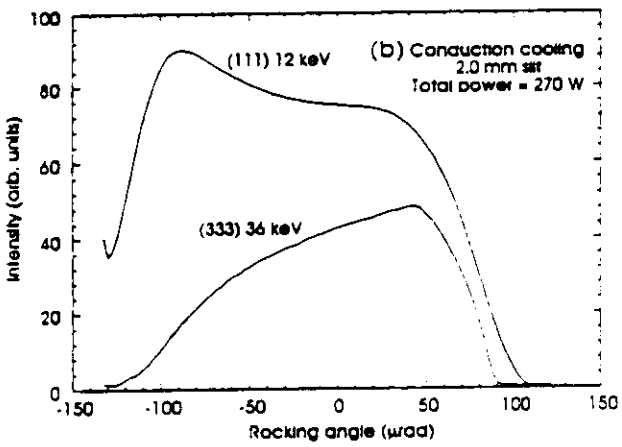

Rocking curves obtained with a crystal cooled by conduction to a water-cooled copper base. The (111) and (333) intensities have been multiplied by different scaling factors. Here (a) shows the low-power results. The (111) 12 keV curve has a full width at half-maximum (FWHM) equal to the theoretical calculation for perfect crystals. The (333) 36 keV curve is slightly broader than the theoretical calculation, which has a FWHM of 2.0 μrad. The high-power results are shown in (b). Severe thermal strain caused grossly deformed rocking curves. Under these conditions, the observed temperature rise of the hot spot on the crystal was 65 °C.

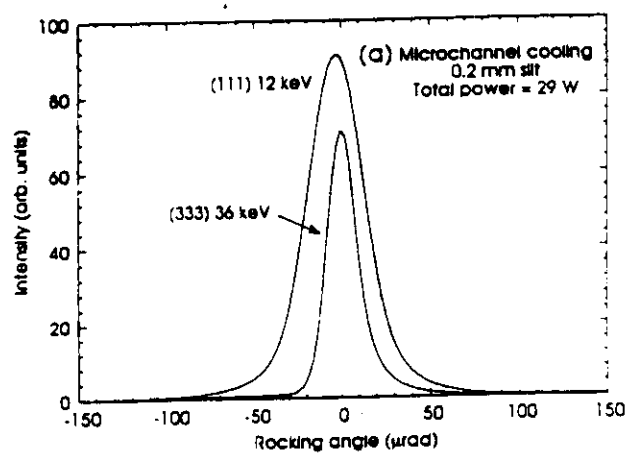

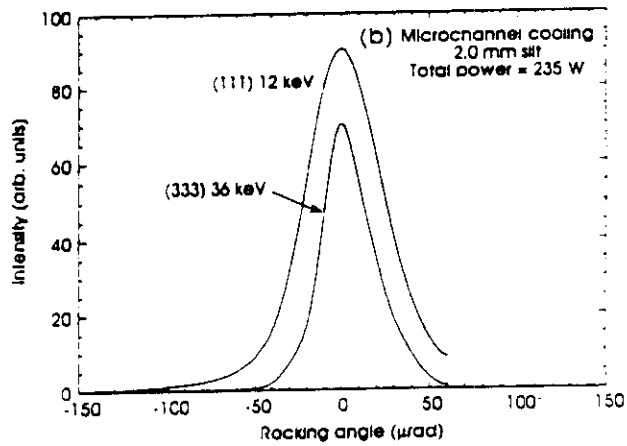

Rocking curves obtained with a microchannel-cooled crystal. Once again, the (111) and (333) intensity values have been multiplied by different scaling factors. The low-power (111) curve in (a) is only slightly broader than the perfect-crystal calculation, though the (333) curve shows the presence of a small amount of permanent strain in the crystal. Under high-power conditions (b), only a small amount of heat-induced strain is indicated. The temperature rise of the hot spot on the crystal under high-power loading was about 5 °C.

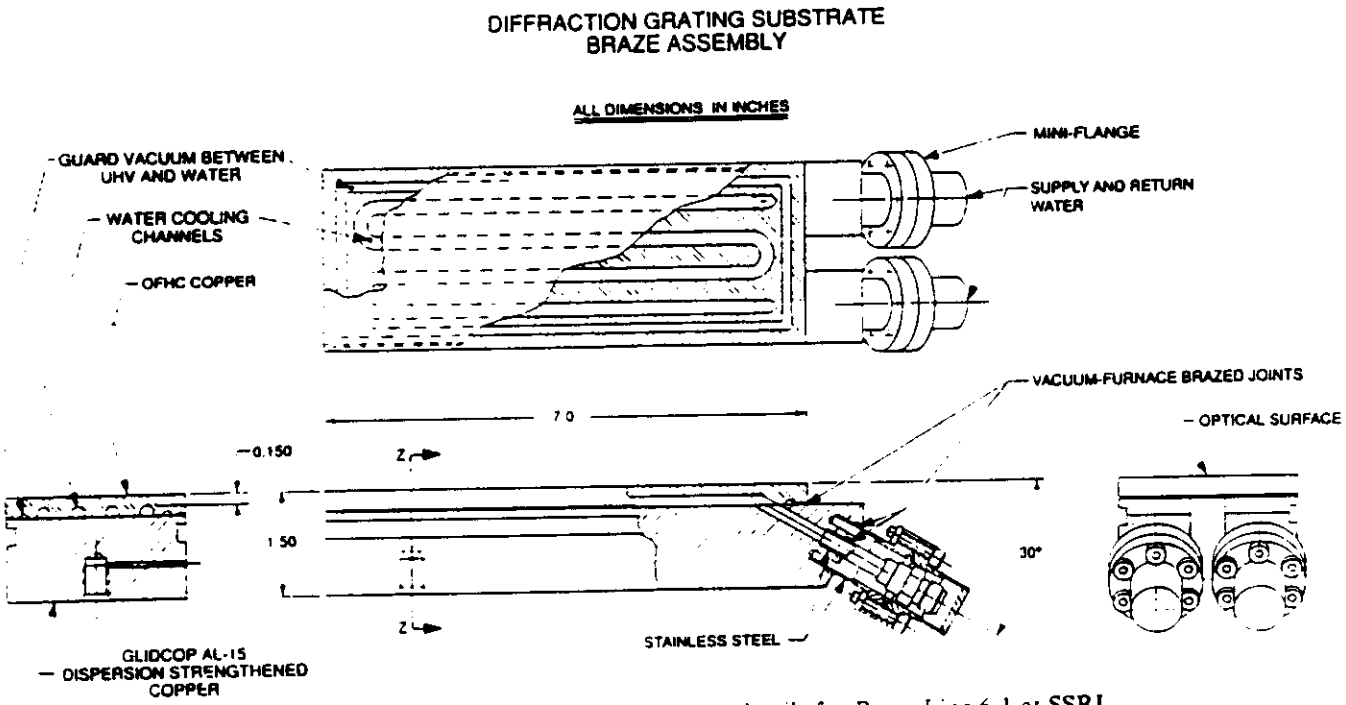

LBL-SGM water cooled grating substrate details for Beam Line 6-1 at SSRL.

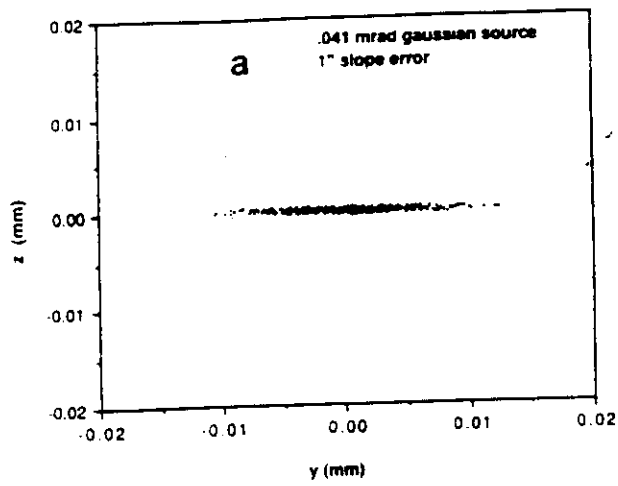

Focal images obtained with 1 arcsec random slope error on mirrors: (a) ellipsoidal mirror

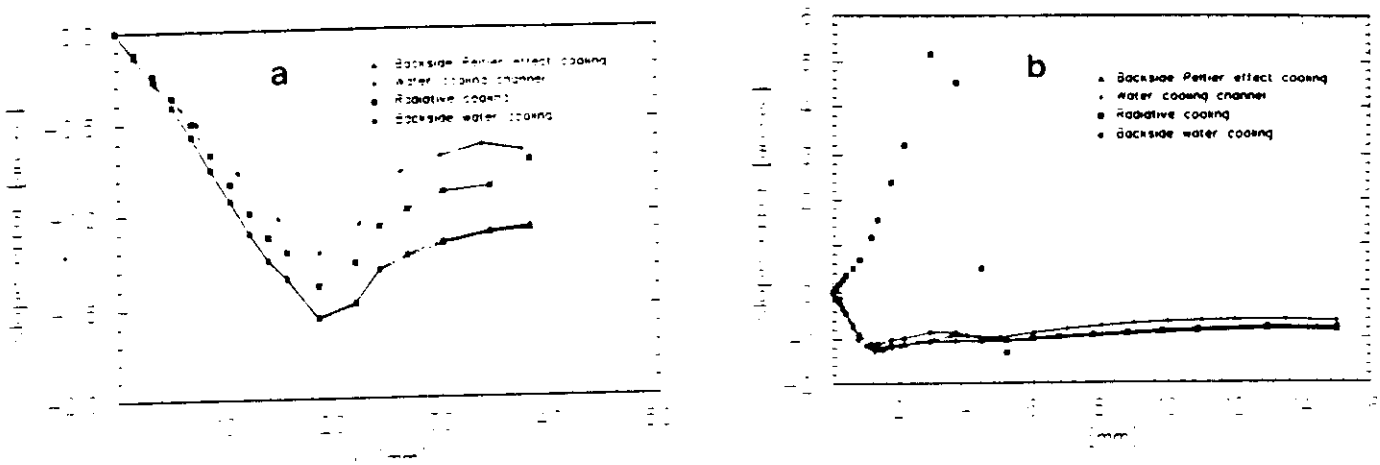

Slope errors on mirror surface for different cooling schemes in (a) tangential direction and (b) sagittal direction.

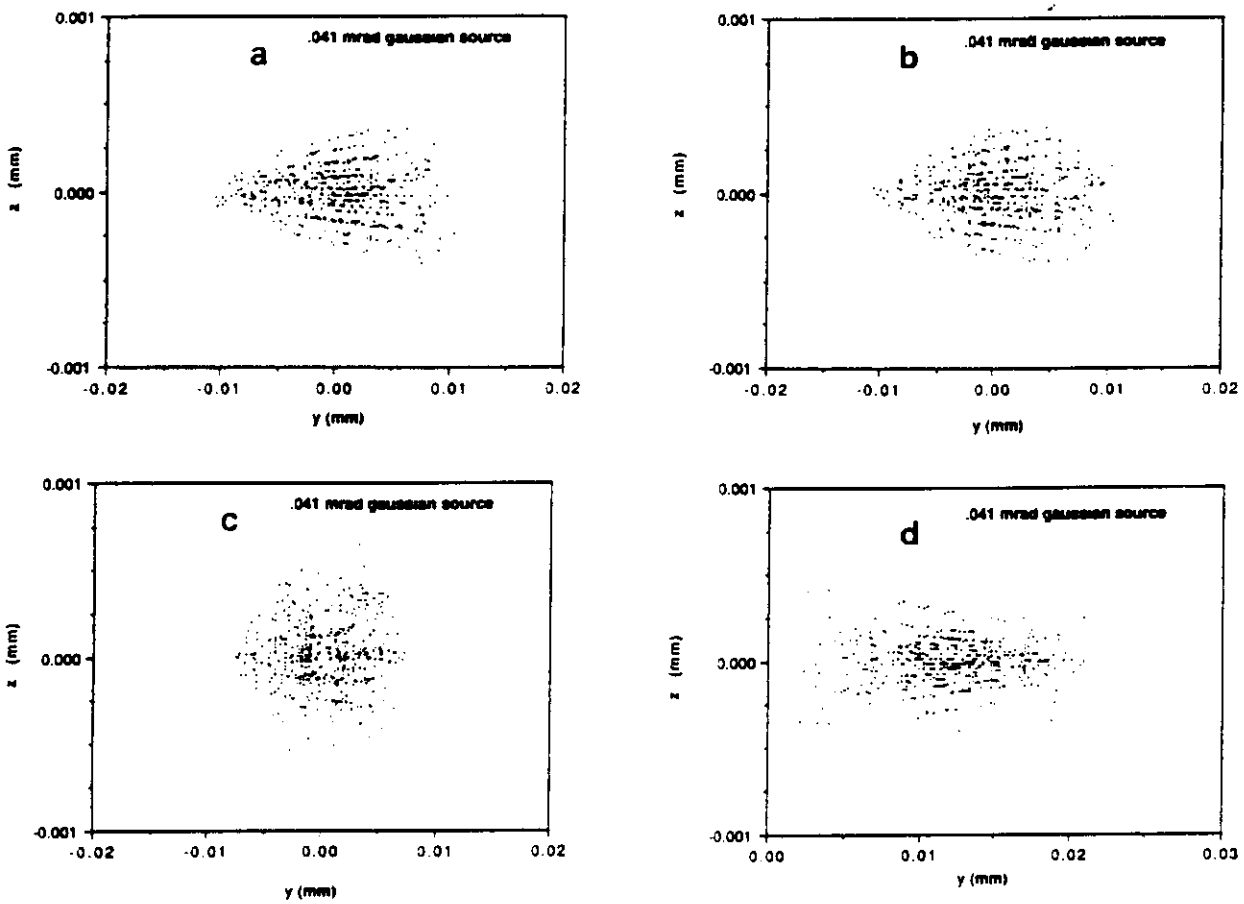

Focal-ray pattern of the ellipsoidal mirror with thermal load only: (a) constant water cooling on back: (b) uniform backside mperature (Peltier effect heat exchanger); (c) water-cooling channel: and (d) radiative cooling.

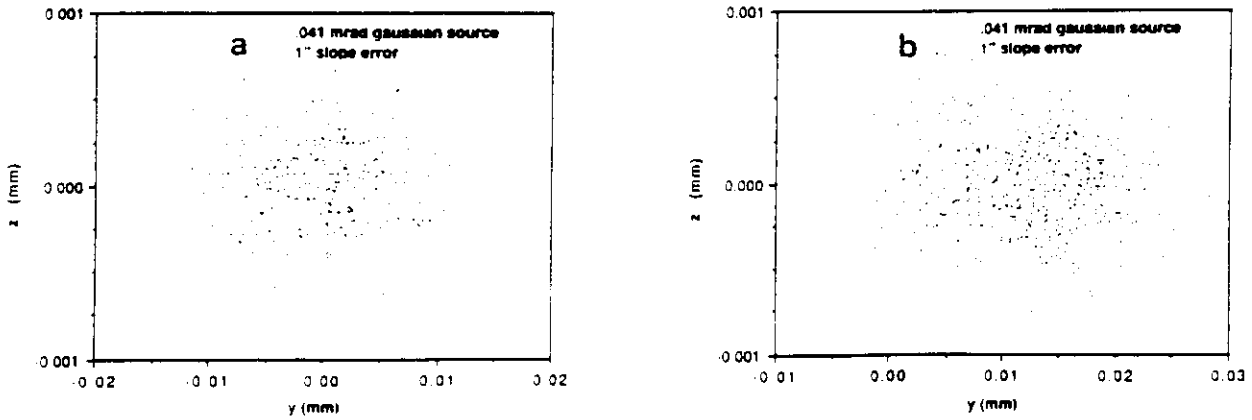

Focal ray pattern of the ellipsoidal mirror with thermal load and 1 arcsec slope error: (a) water-cooling channel: (b) radiative cooling.

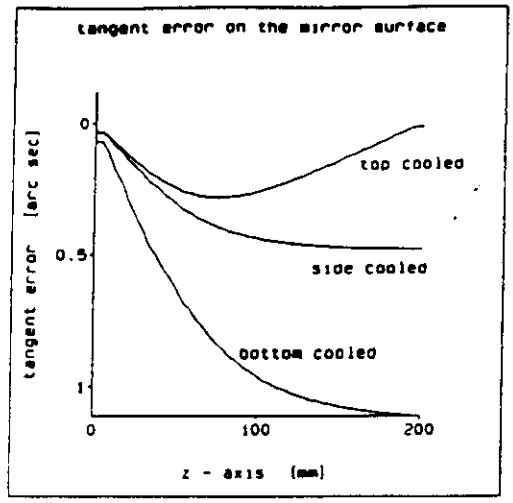

The three test cooling cases. Shown is the tangent error vs position on the mirror surface. Only one half of the mirror is shown.

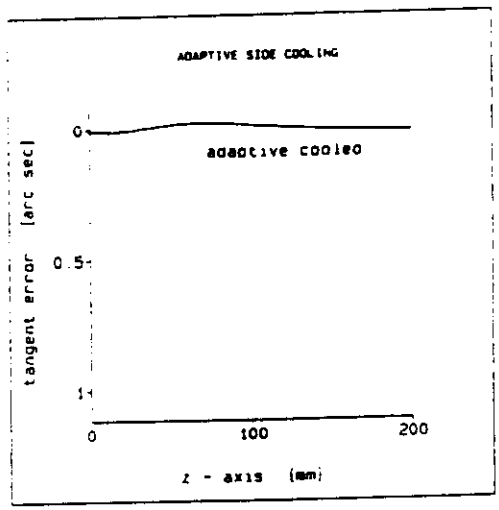

Meridional tangent errors on the adaptively cooled mirror. The tangent errors are much smaller than the 0.1 arcsec rms tangent error and hence do not deteriorate the focusing properties of the mirror.

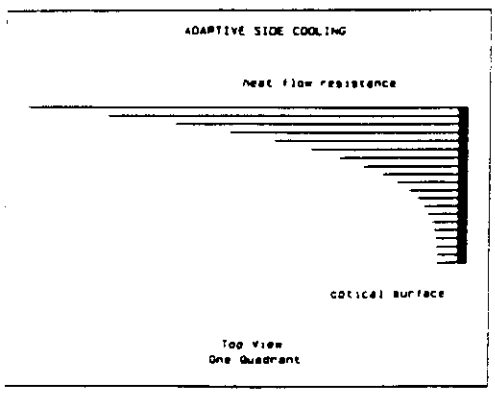

FEM analysis for adaptive side cooling showing the heat flow pattern necessary to produce laminar isotherms parallel to the long sides of the mirror. Note that the lines projecting out from the side of the mirror quadrant are proportional to the resistance to heat flow.

Liquid Gallium cooling

Favourable properties

- High thermal conductivity
- High specific heats
- Large range of working temperatures
- Low vapour pressure
- Room temperature melting point

Drawbacks

- High reactivity with other metals (but not with silicon and stainless steel T < 400 °C)
- Liquid metal pump(*)
  - high pressure
  - moderate flow rate

(*) Film coefficient for liquid metal flow (Baker and Tessier):

$$h = A_1 \frac{k}{d} + A_2 \frac{k^{0.6}}{d^{0.2}} \frac{C_v^{0.4}}{\nu^{0.8}} V_a^{0.8}$$

k thermal conductivity; d hydraulic diameter; ν kinetic viscosity; C_V volume specific heat; V_a fluid velocity, A_1, A_2 constants with values near 1 (empirically determined).

Properties of cooling fluids

Coolant	M.P. [°C]	B.P. [°C]	V.P. [mm Hg]	k [W·cm^{-1}·K^{-1}]	Cv [J· cm^3]	ν [p·g^{-1}]	$\frac{k^{0.6}C_v^{0.4}}{\nu^{0.8}}$
Ga (50°)	29.8	2071	$<10^{-14}$	0.33	2.4	0.0026	90.0
H_2O (20°)	0.0	100	0.17	0.006	4.12	0.0100	5.34
N_2 (–170°)	–210	–196	$7.5\ 10^3$	0.0014	1.6	0.0021	4.57
C_3H_8 (–170°)	–187	– 42	$3.1\ 10^{-3}$	0.0020	1.4	0.0075	1.38

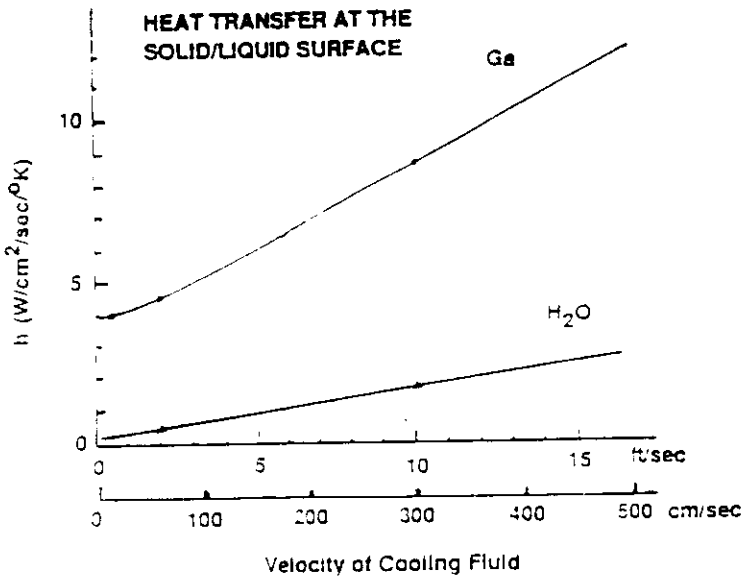

Plot of h, the heat transfer coefficient, for liquid Ga (upper curve) and for water (lower curve) as a function of cooling-fluid flow rate in an 0.5-cm-diameter channel.

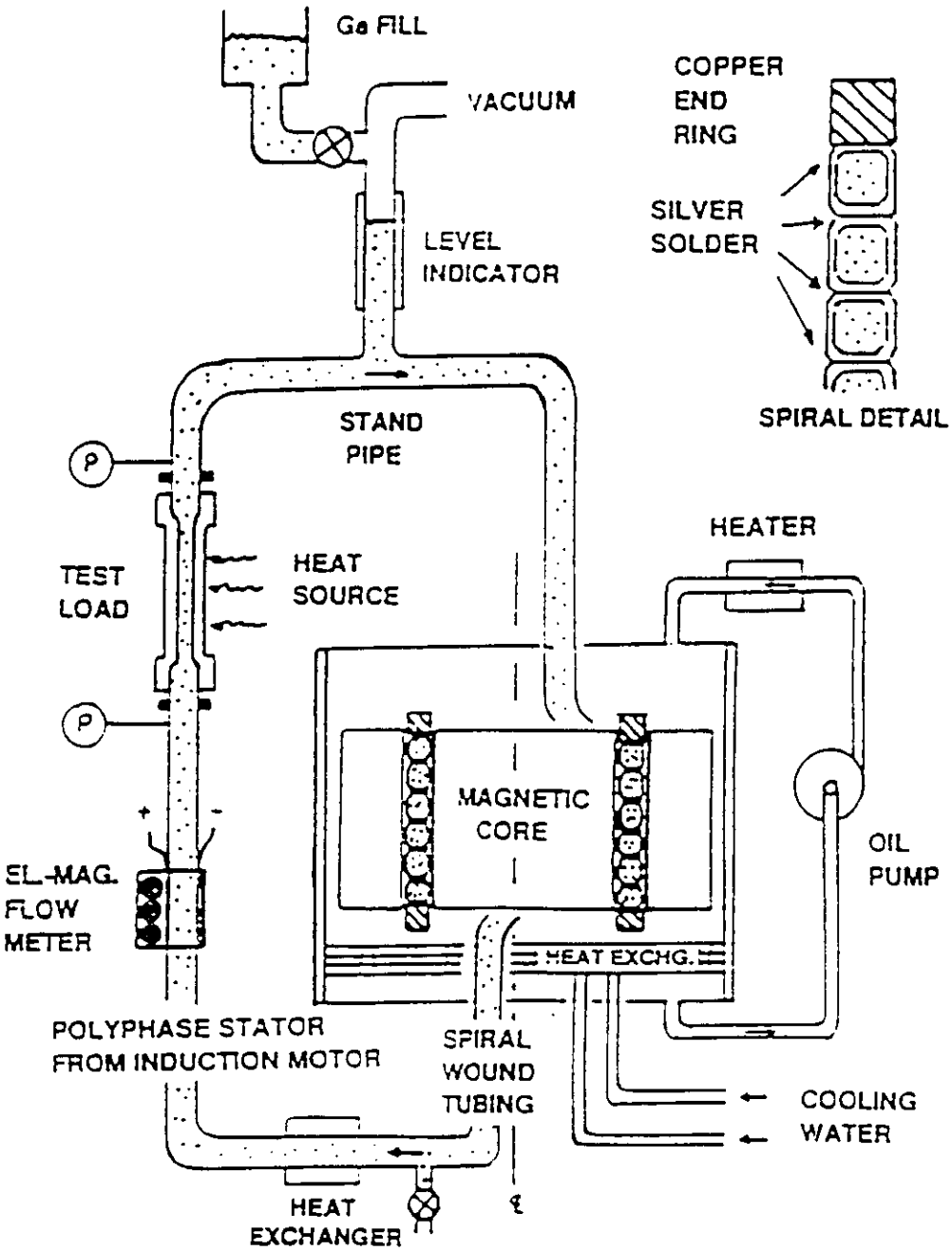

Schematic drawing of the gallium pump.

Heating the crystal

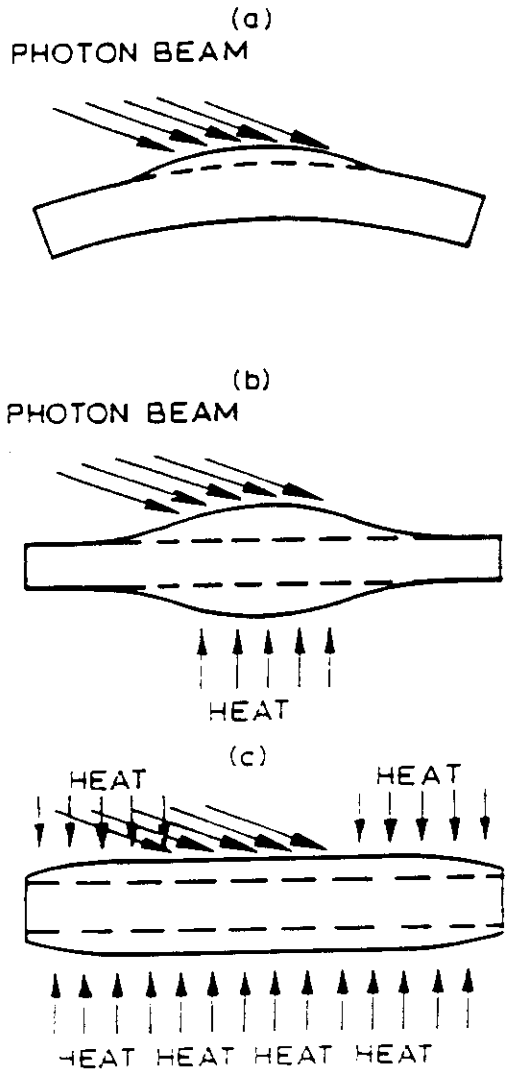

Distortion in the crystal surface with large heat loads and possible solutions. (a) Absorbed photon beam "warps" crystal; (b) with backside auxiliary heating, the bowing can be minimized; (c) best solution, add heat to both the front and backsides to unstress the crystal (Smither et al. 1988).

Cryogenic Cooling

Properties of some crystals (Si, Ge, etc.)

- Thermal conductivity k increases when the temperature decreases (up to few tens of K degrees).

  ==> reduction of ΔT

- Thermal expansion coefficient α decreases when the temperature decreases. It goes to 0 at absolute zero and again at 125 K for Si and 50 K for Ge. Between these temperatures α is negative.

  ==> reduction of d-spacing non uniformity

For cooling a Si crystal the fluid must have the following properties:

a) liquid phase between 80 and 120 K

b) good cooling characteristics

c) non-toxic, non-flammable

==> good choice liquid N_2

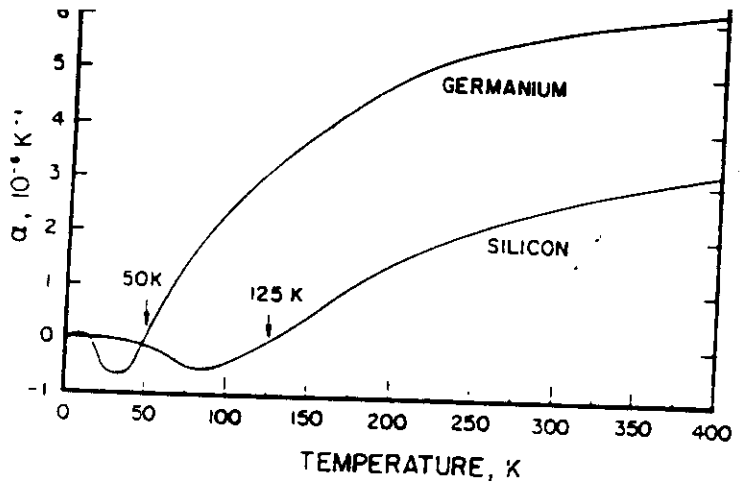

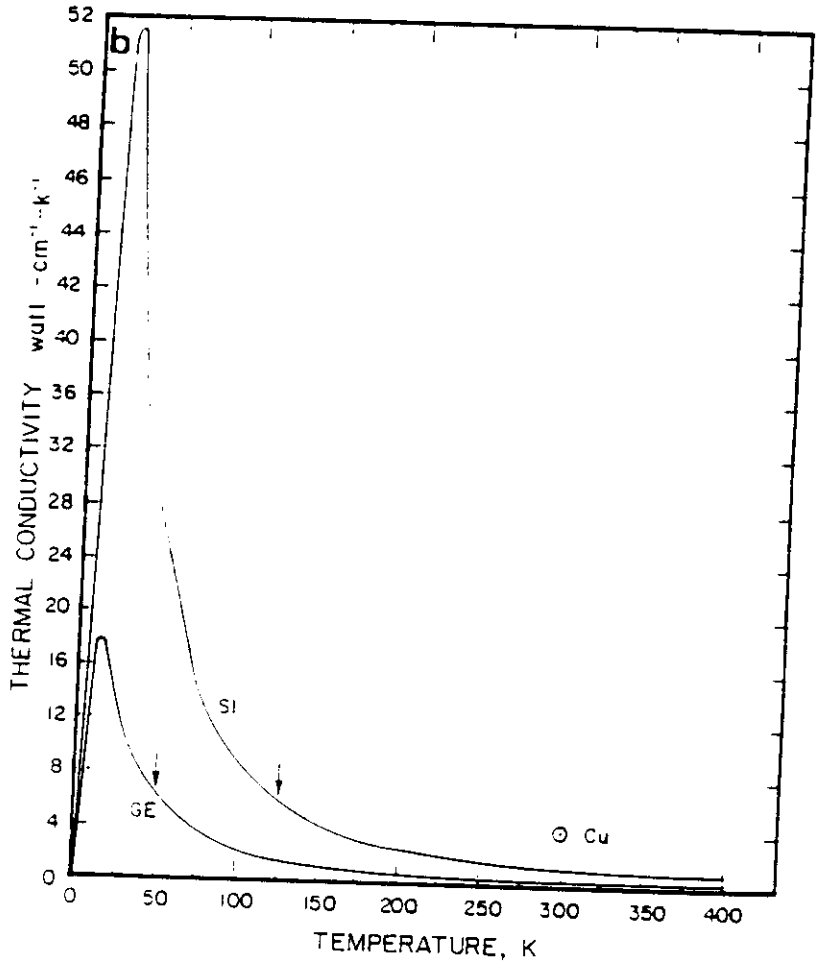

Thermophysical properties of undoped silicon and germanium. (a) Coefficient of thermal expansion goes to zero at 0 and again at 50 K (Ge) and 125 K (Si). (b) Thermal conductivity is greatly improved by operation at low temperatures (Bilderback 1986).

CRYOGENIC COOLING OF SILICON CRYSTALS

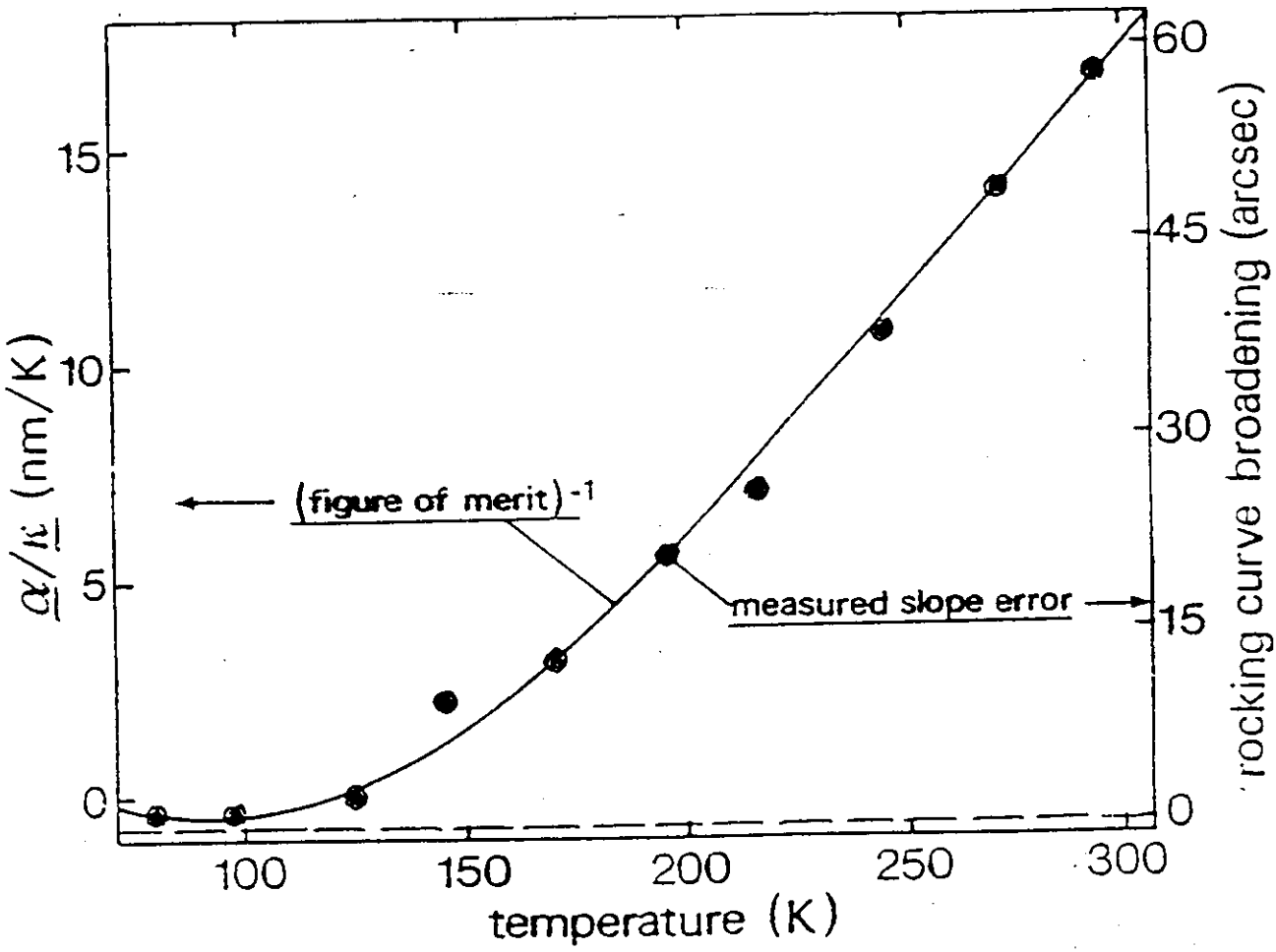

The ratio of thermal expansion over thermal conductivity and the measured (333) rocking curve broadening (dots) as a function of temperature.
Power density: 150 W/mm2. Total power: 75 W.

CRYOGENIC COOLING OF SILICON SINGLE CRYSTALS

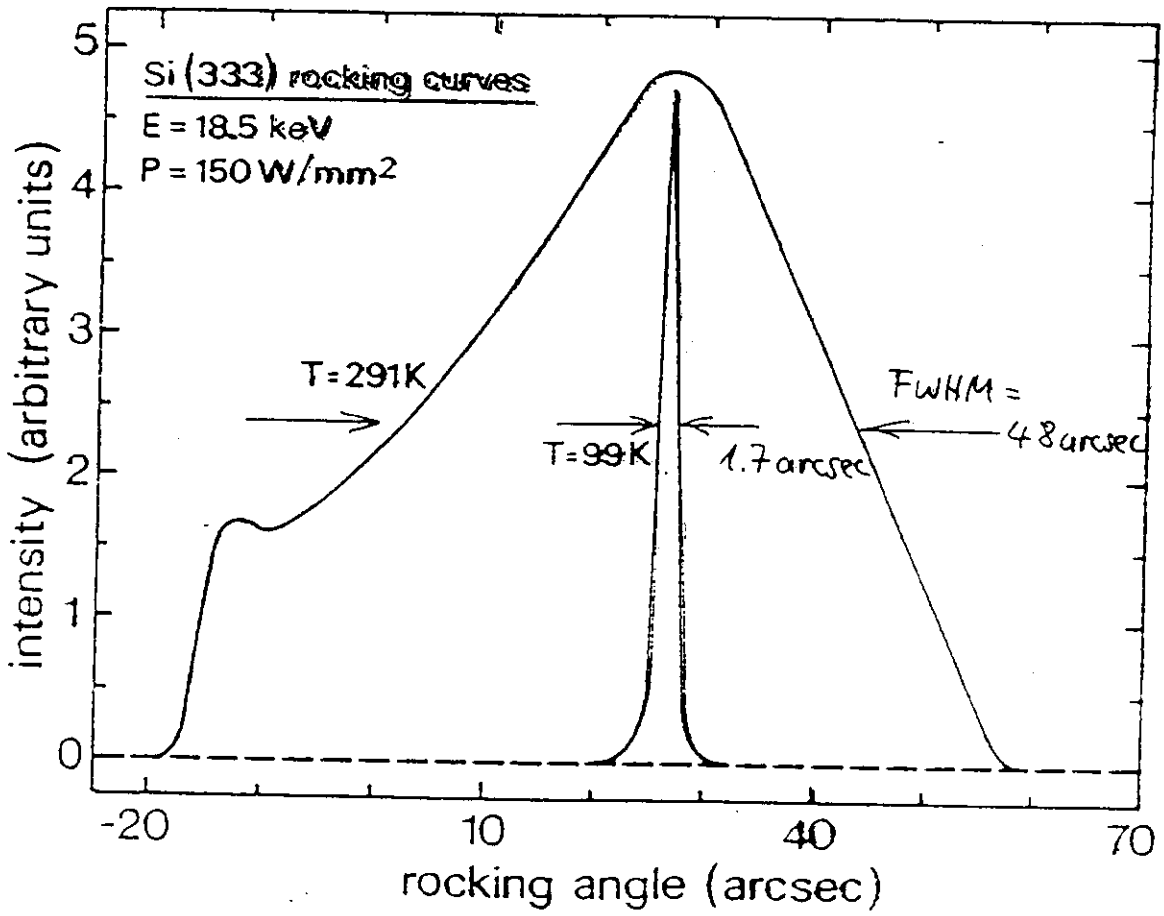

Rocking curves recorded at room and at low temperature. The intensity scale and peak position are not the same for the two profiles.

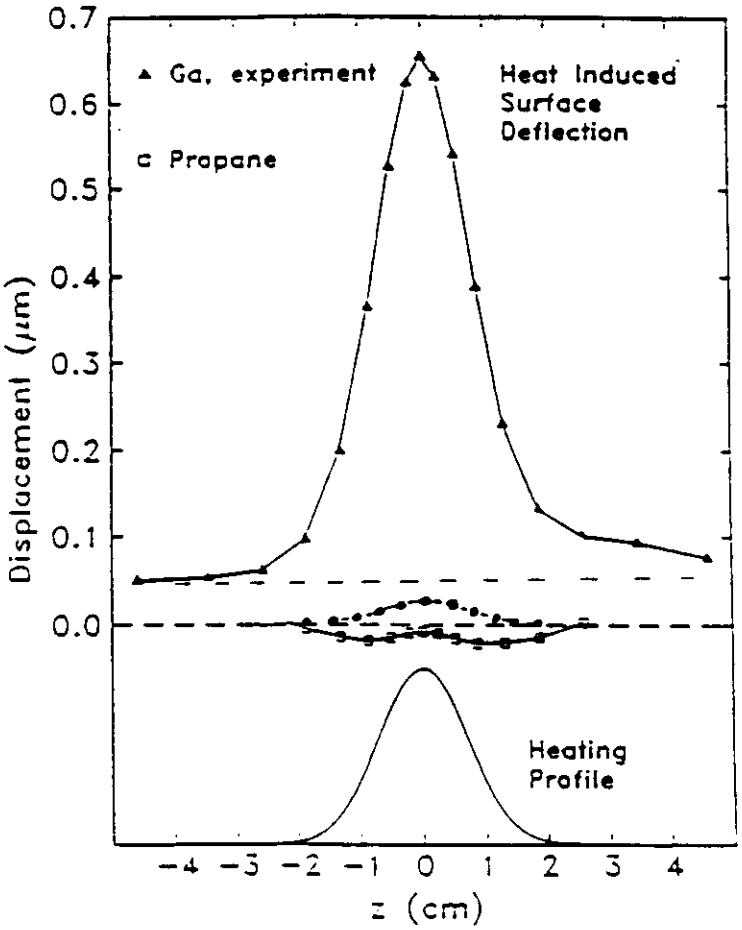

Calculated surface displacement (vertical) of the slotted crystal in the ANL/CHESS undulator beam for experimental conditions in the undulator test with liquid-gallium cooling (triangles), liquid propane (squares) and the limit for either liquid-gallium or water cooling (circles).

Thin crystals

- Thermal bending is independent on thickness D.
- Thermal bump increases as D^2.
- d-spacing variation increases as D.
- High of the bump for thin materials depends inversely on *h*.

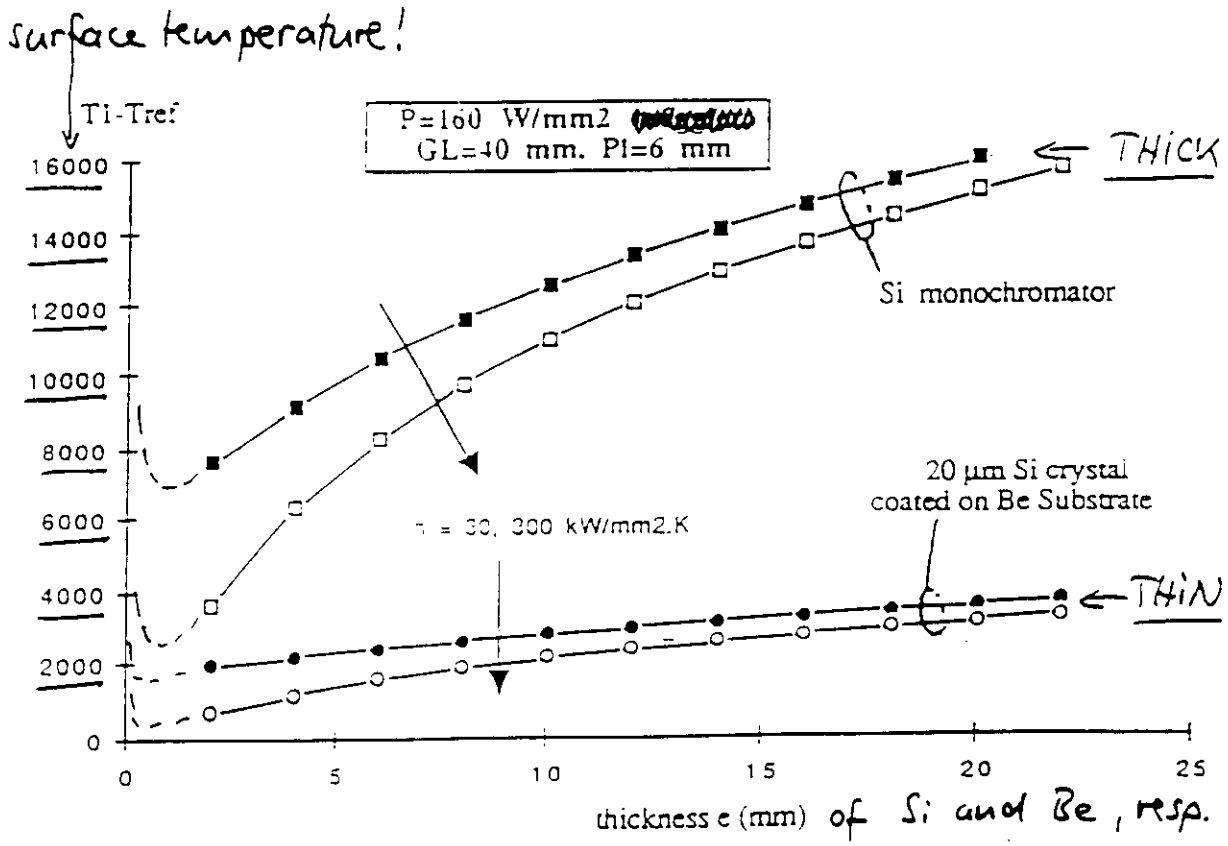

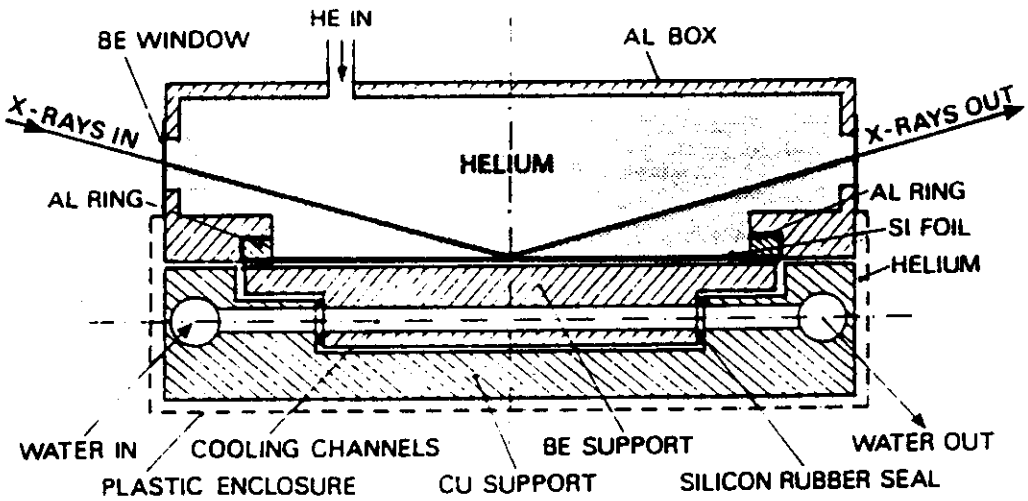

Schematic drawing of the cooled thin silicon crystal assembly. For the sake of clarity, the spacing between the Si foil and Be support was exaggerated, but in reality, both touch each other. When the ring stretches the foil it bends downward at its periphery and a gap is formed between the Si foil and the Be substrate (dotted line).

Adaptive optics

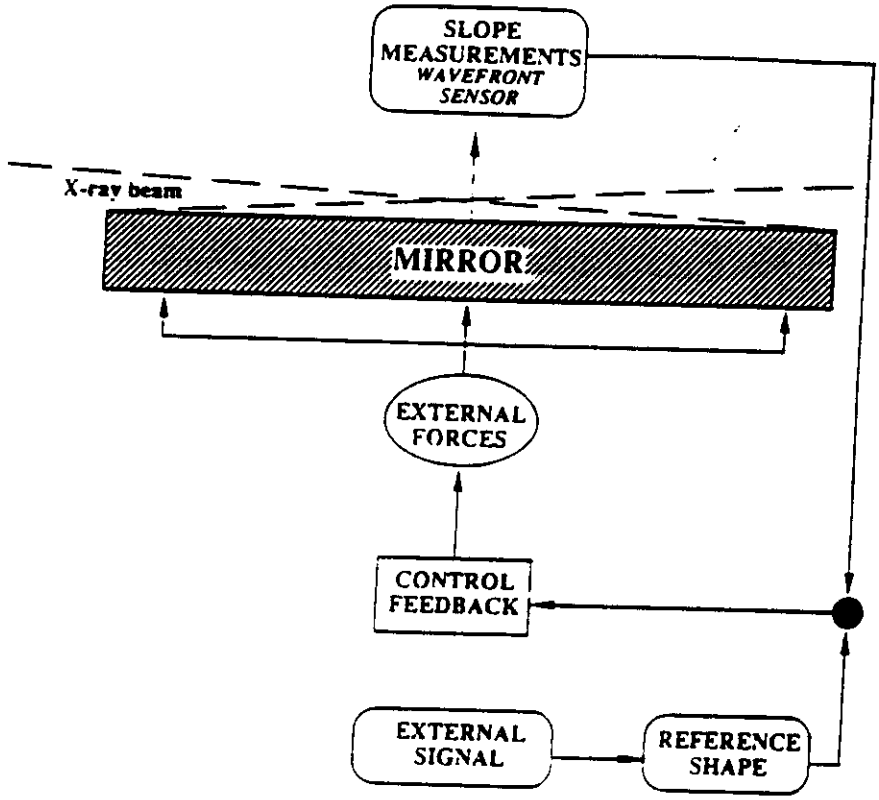

General principle of an adaptive mirror.

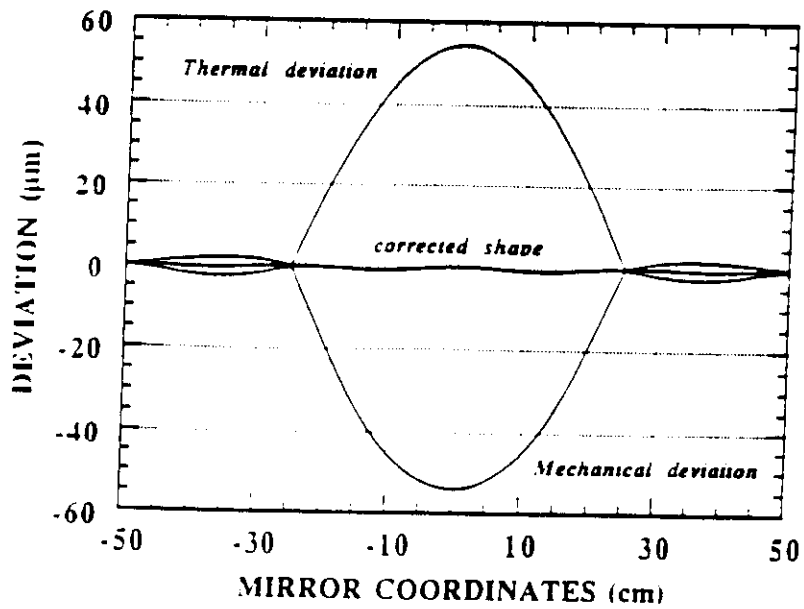

Minimization of the thermal deformation by a mechanical correction by using a set of 11 actuators.

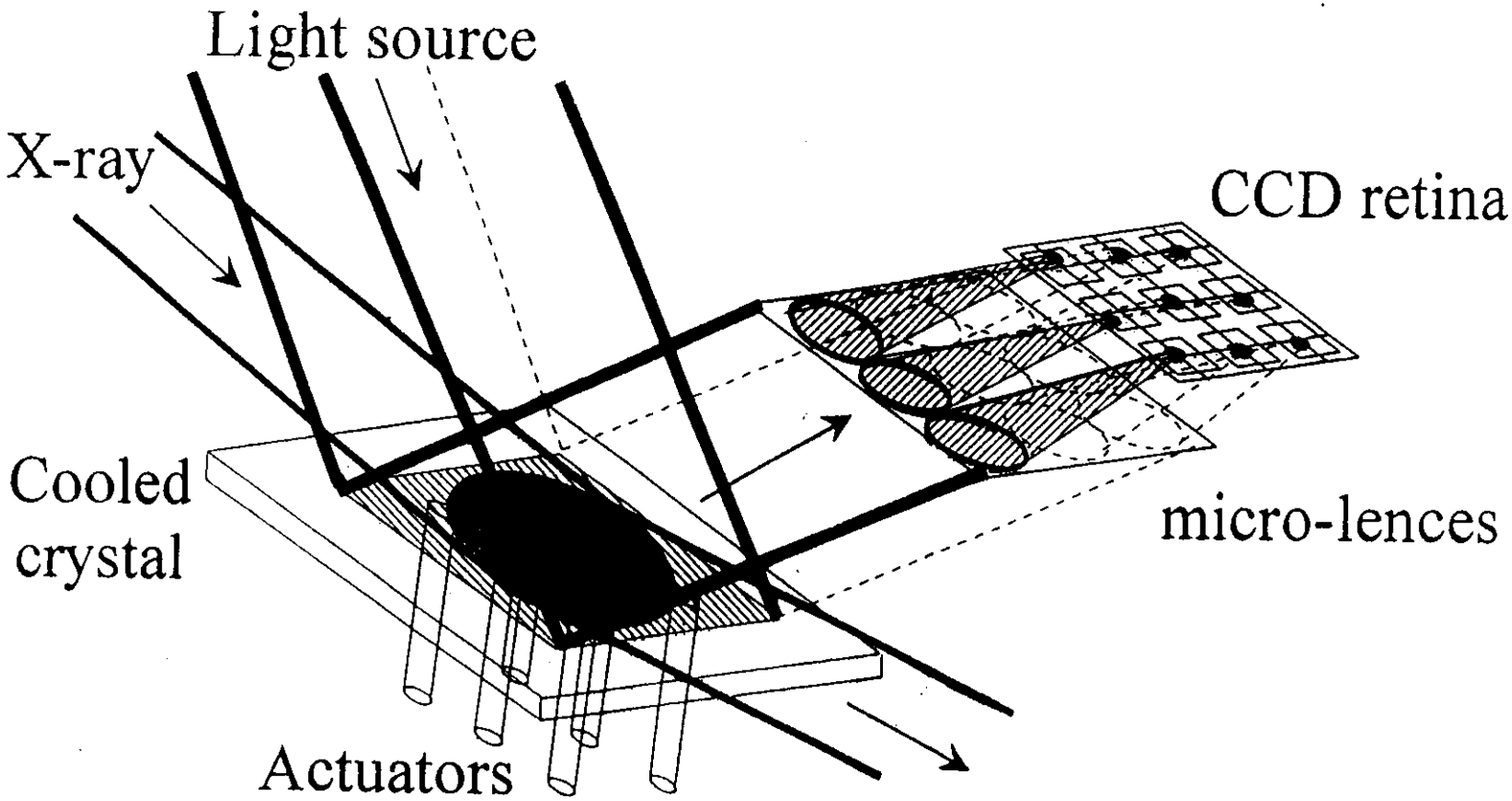

Wavefront sensor principle

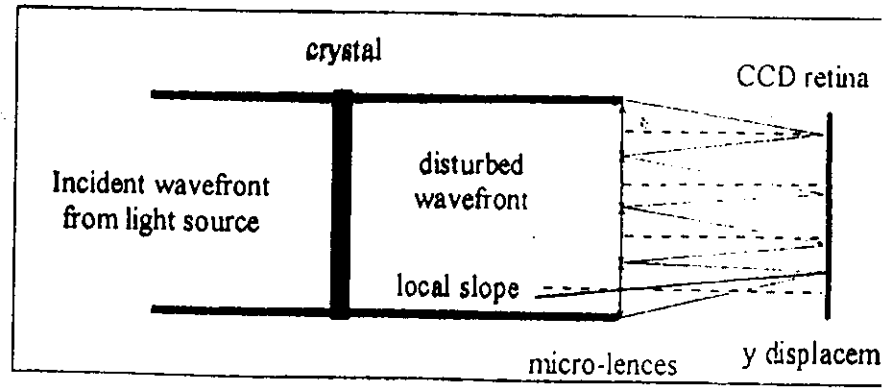

ADAPTIVE SYSTEM

slope ± 50 μrad
actuator voltage ± 400 V

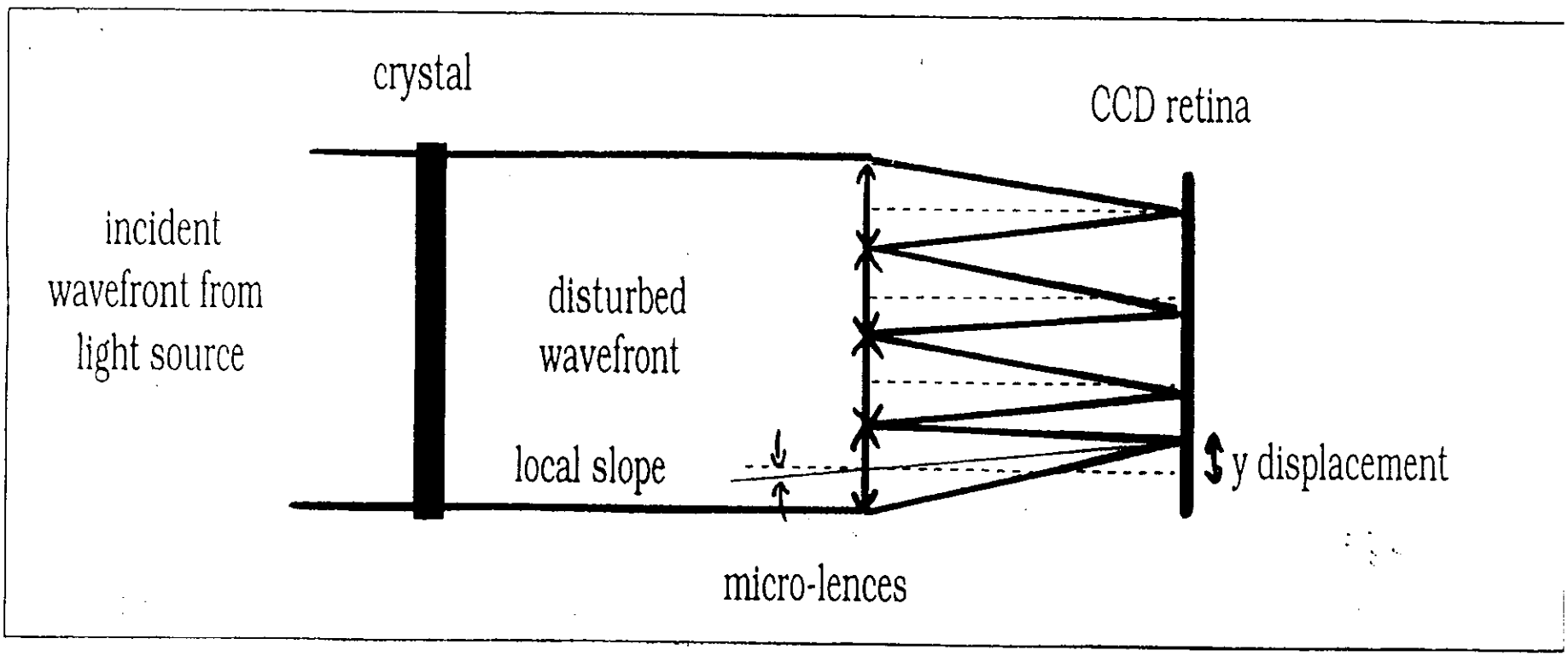

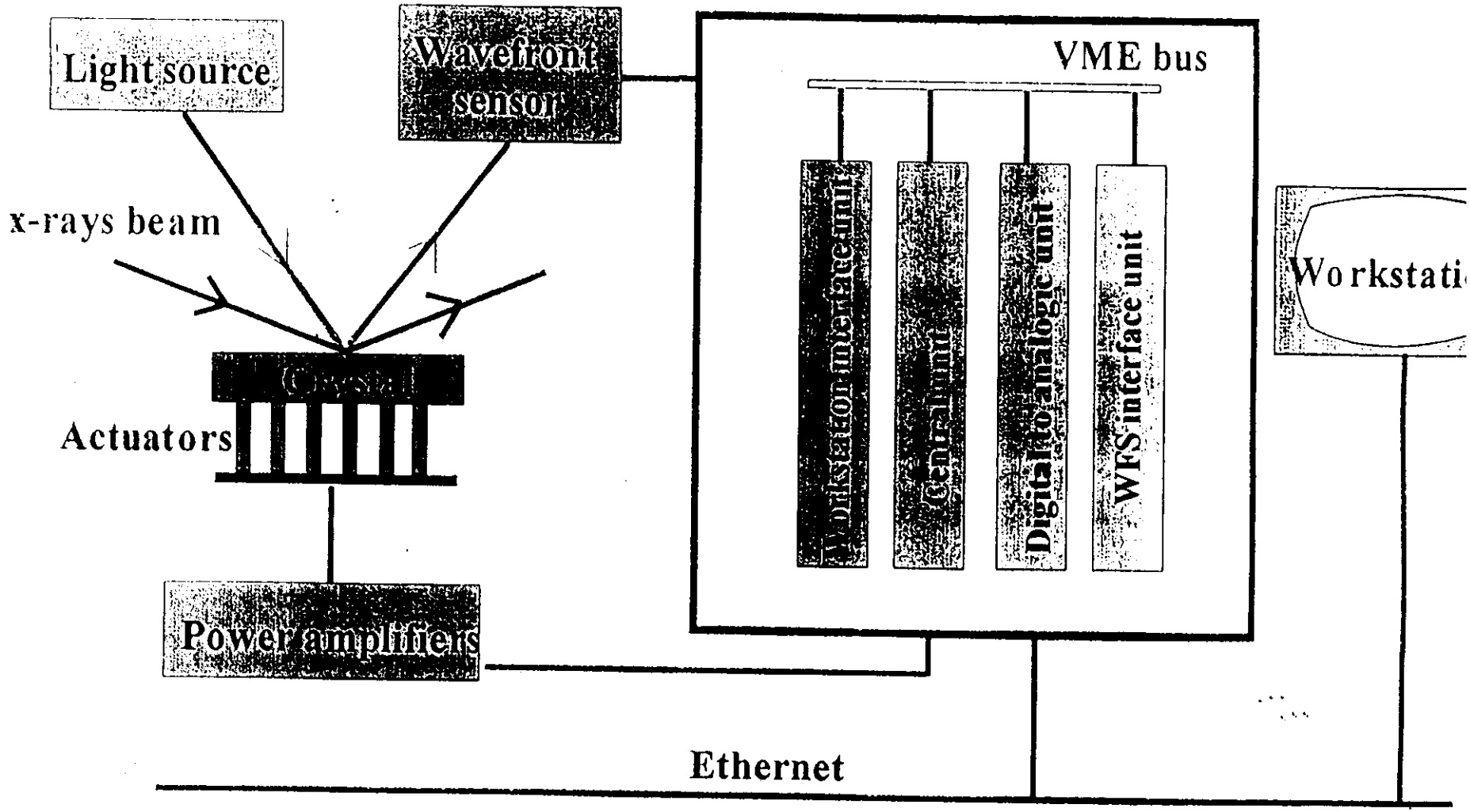

Adaptive crystal system hardware

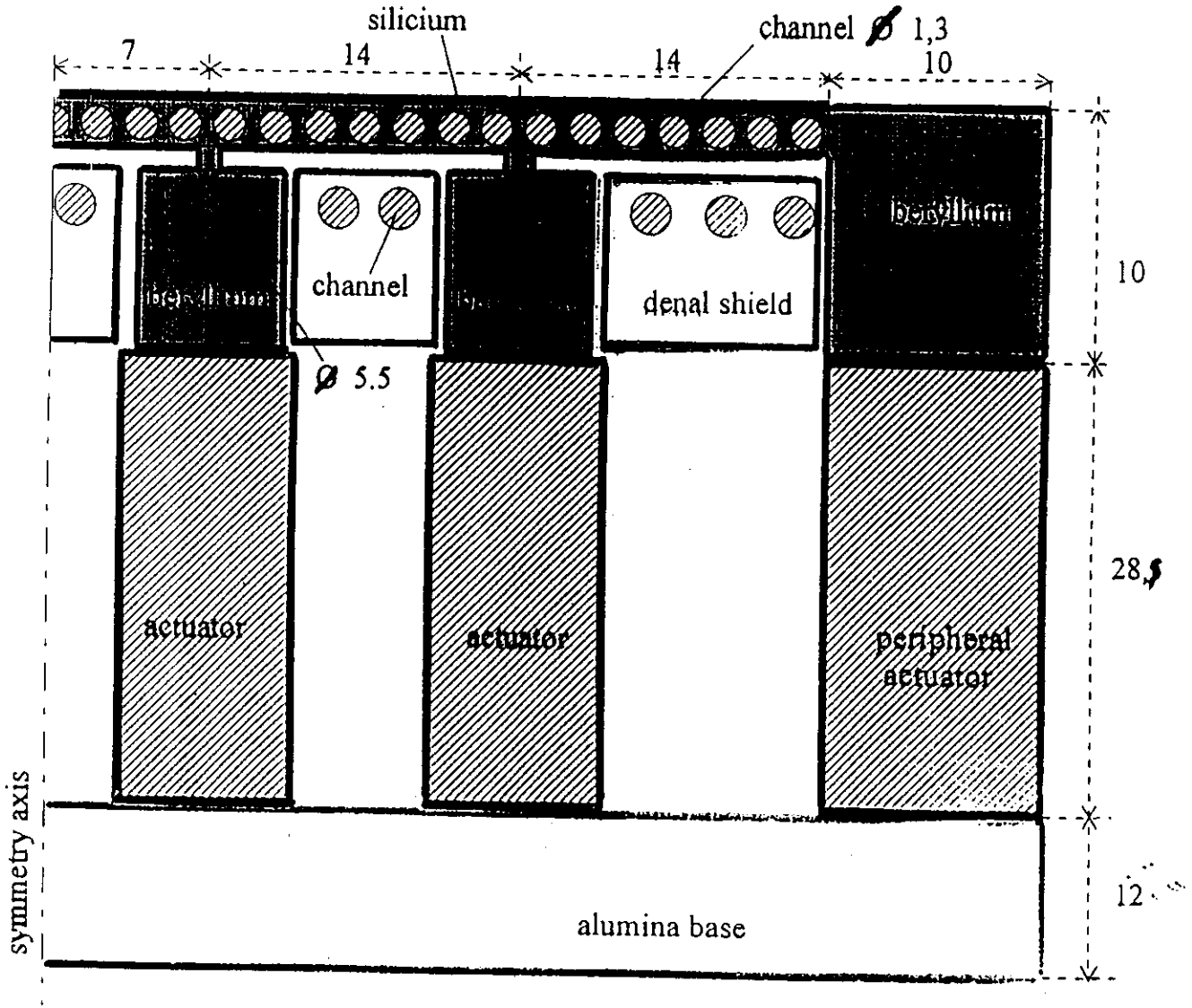

Adaptive cooled crystal schematic

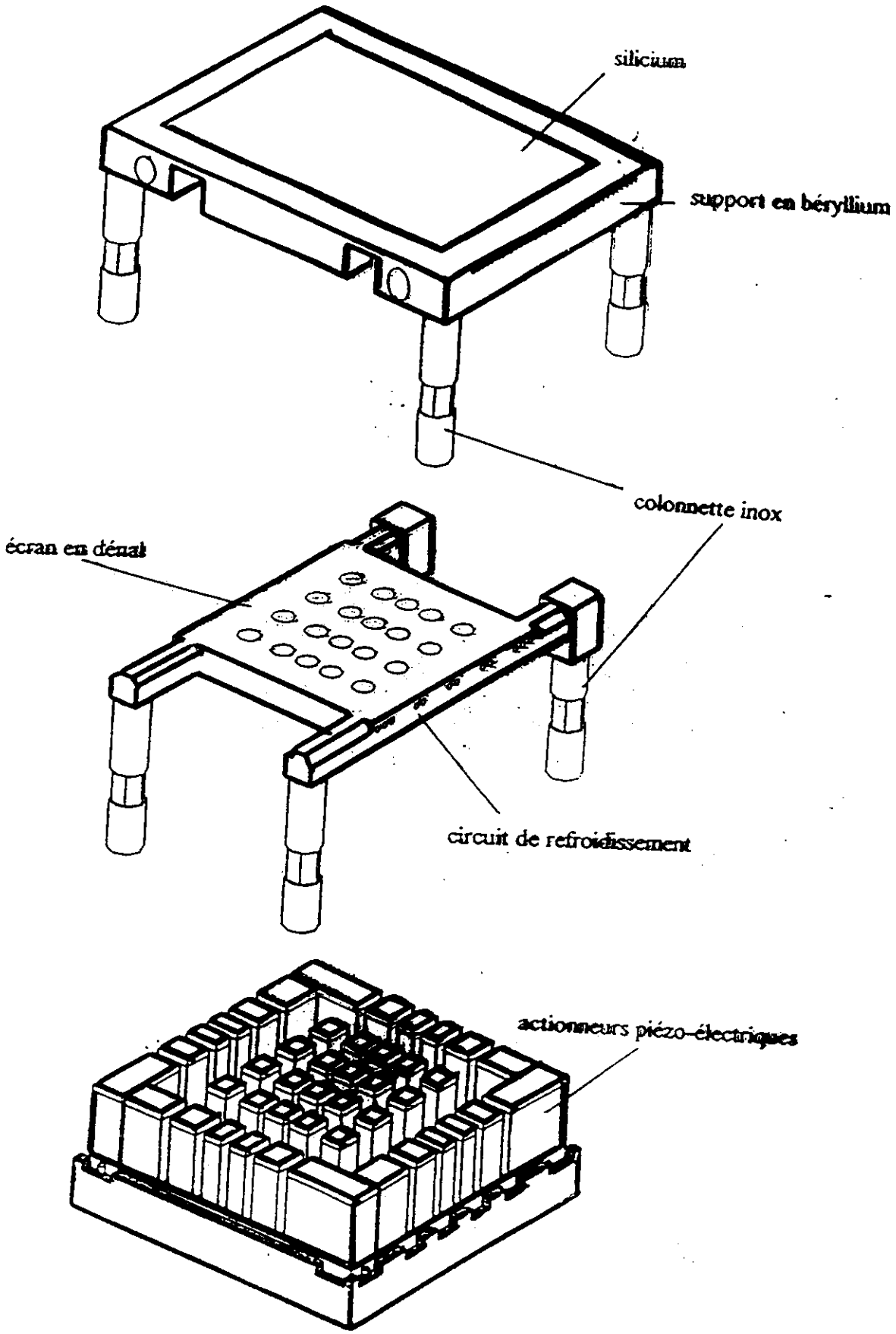
silicium
support en béryllium
colonnette inox
écran en dénal
circuit de refroidissement
actionneurs piézo-électriques

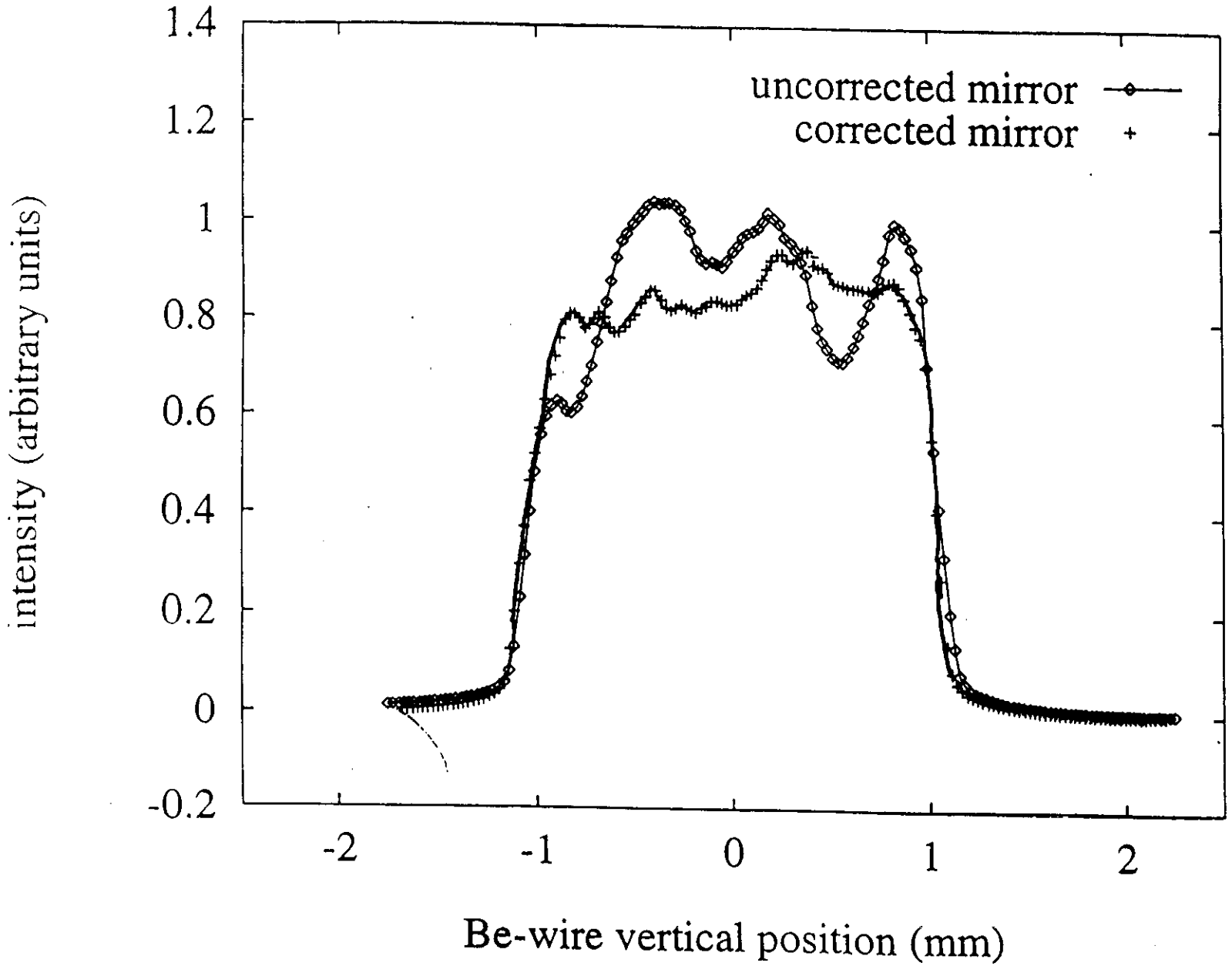
uncorrected mirror
corrected mirror
intensity (arbitrary units)
Be-wire vertical position (mm)
1.4
1.2
1
0.8
0.6
0.4
0.2
0
-0.2
-2
-1
0
1
2

MEASURED BEAM PROFILE

*Gap=80mm, I=100mA, θ=3mrad, Slits=40*2mm²*

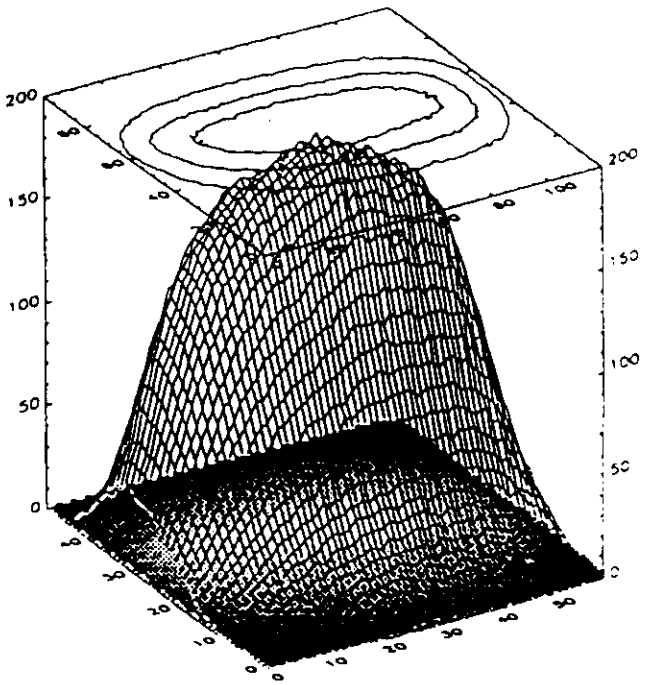

uncorrected: 2.39mm

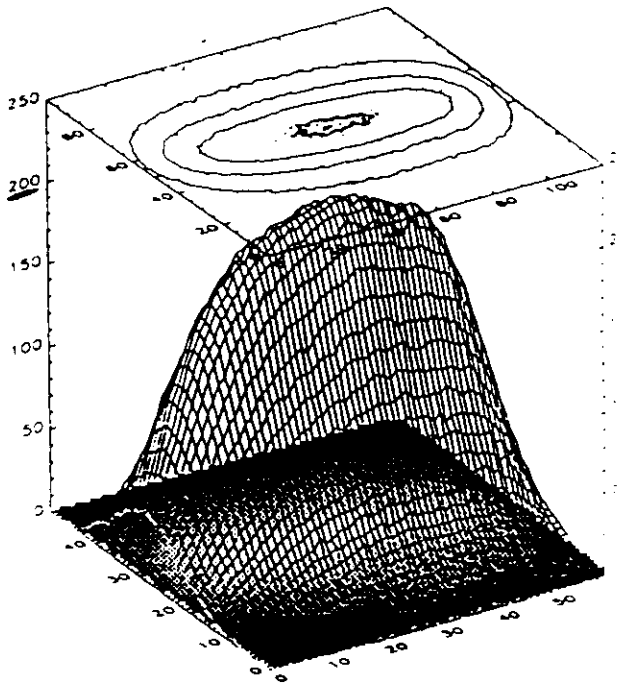

flat: 2.17mm

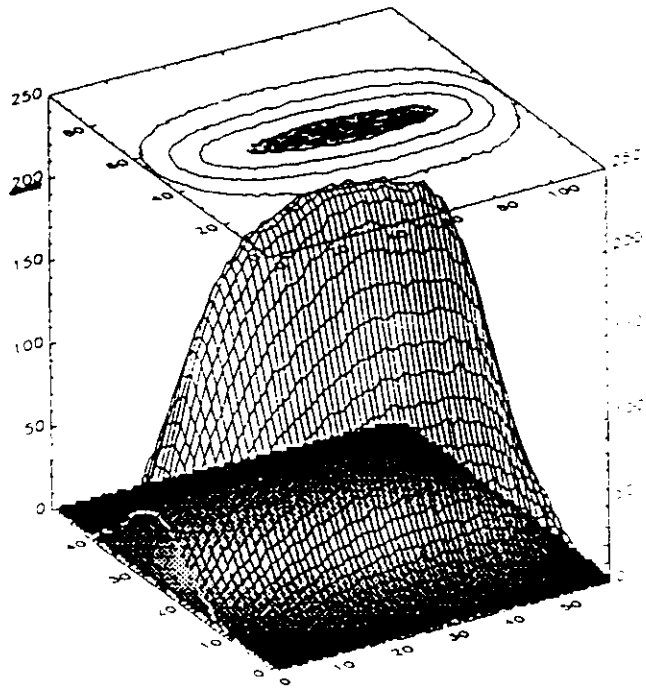

parabolic: 1.94mm

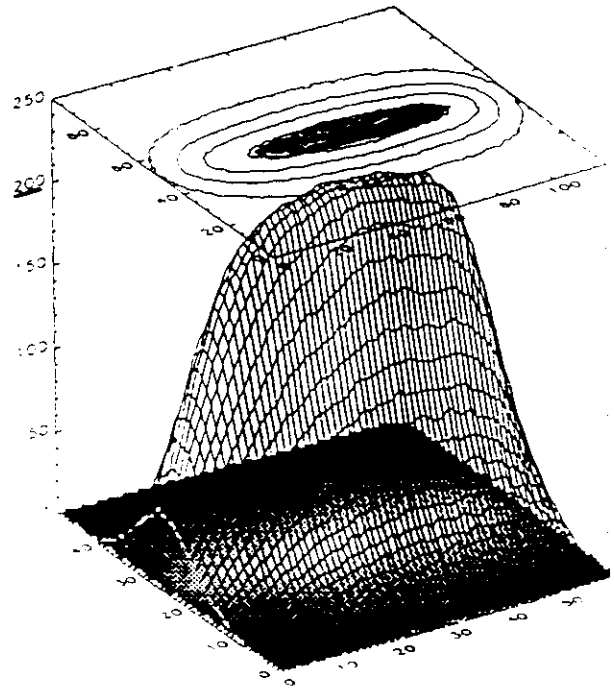

elliptical: 1.82mm

1-) Some of the features that make thin diamond attractive as a monochromator

- Diamond properties :

- Excellent figure of merit (K/α) at room temperature, (the thermal conductivity of pure diamond is more 15 times that of silicon and about 6 times that of copper),

- Absorbs less radiation than silicon (lower Z material)

- Thin crystals:

- Because the absorption depth is much larger than the extinction depth, most of unwanted radiation is transmitted through by choosing a thin crystal => less power load.

- A thin diamond crystal can be obtained by cleaving along (111) or (100) diffraction planes, and reasonable size, suitable for undulator beam, can be available (typically 1 cm^2 area or less, and 0.5 mm thick,) in natural or synthetic form.

3) Monochromator design and analysis

a. The geometry and the cooling scheme

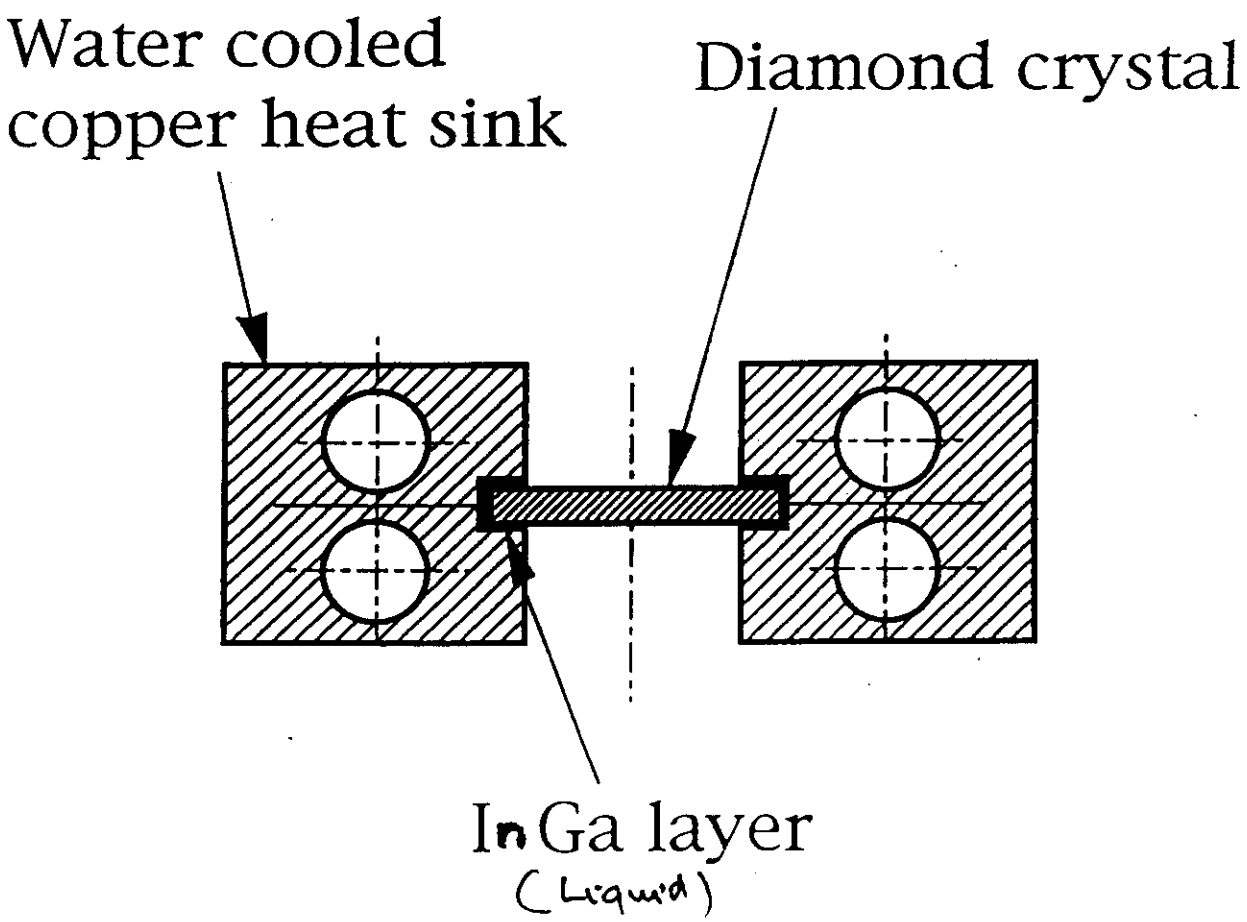

2-) Cooling schemes

• Two possible tested arrangements for cooling a thin diamond crystal:

a) <u>indirect cooling of the crystal at the edges (A. Freund-ESRF, J. Als-Nielson)</u>

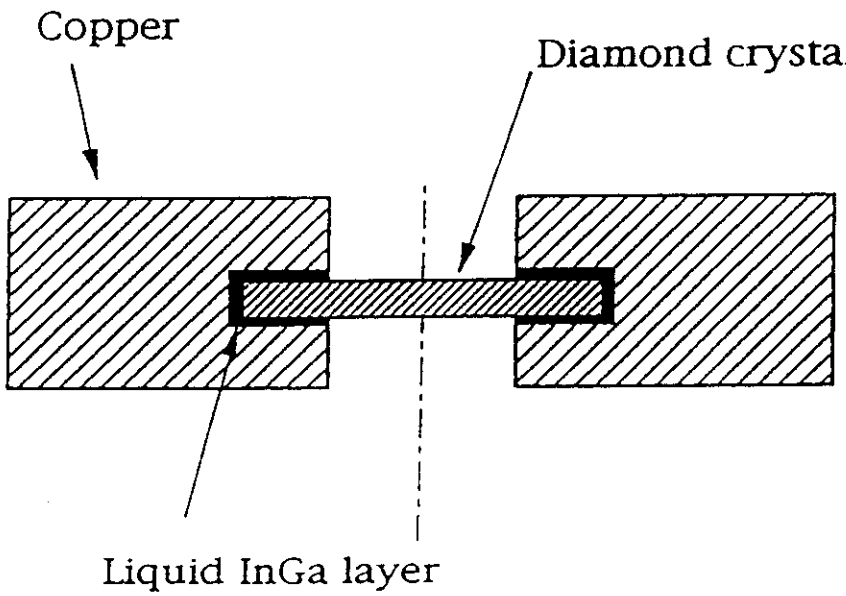

- Advantages:

- Small temperature gradient across the crystal thickness-> minimum slope due to bending

- Strain-free mounting is obtained by using a thin layer of liquid InGa as heat transfer media between the crystal and the heat sink, thus allowing a free expansion.

b) Jet cooling (L. Berman, and M. Hart)

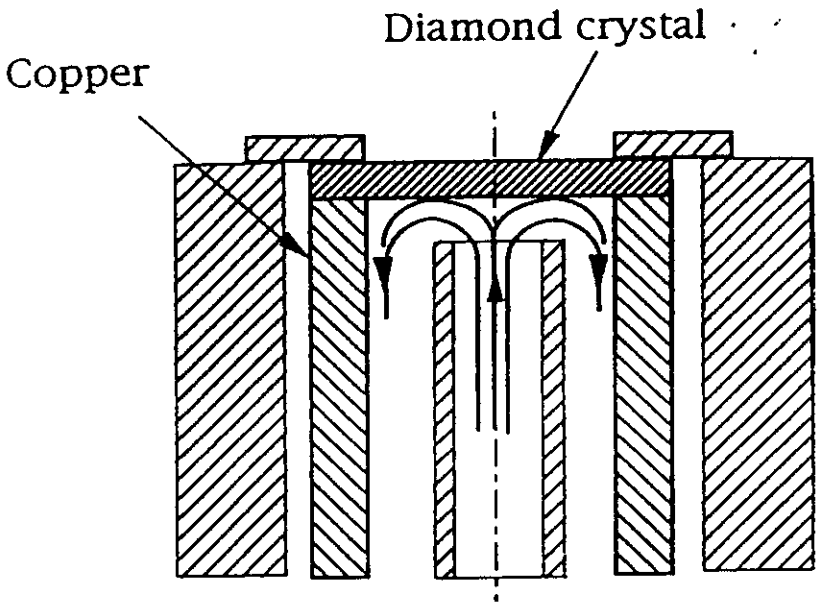

The crystal is clamped at the edges to a copper insert and cooled directly at the back => combination of edge cooling and direct back cooling.

Diamond Crystal Characterization

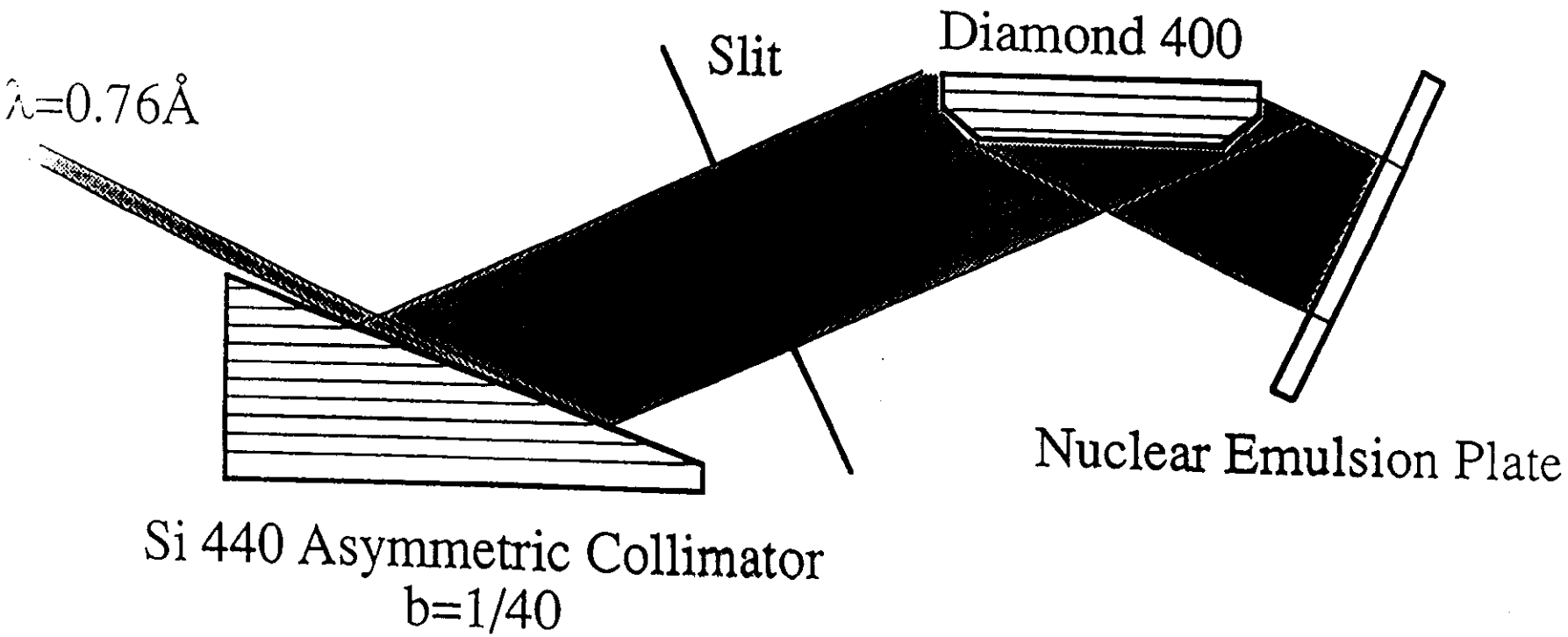

W - U

PG-PM 250 - 2000 eV

Si (111) 2500 - 8000 eV

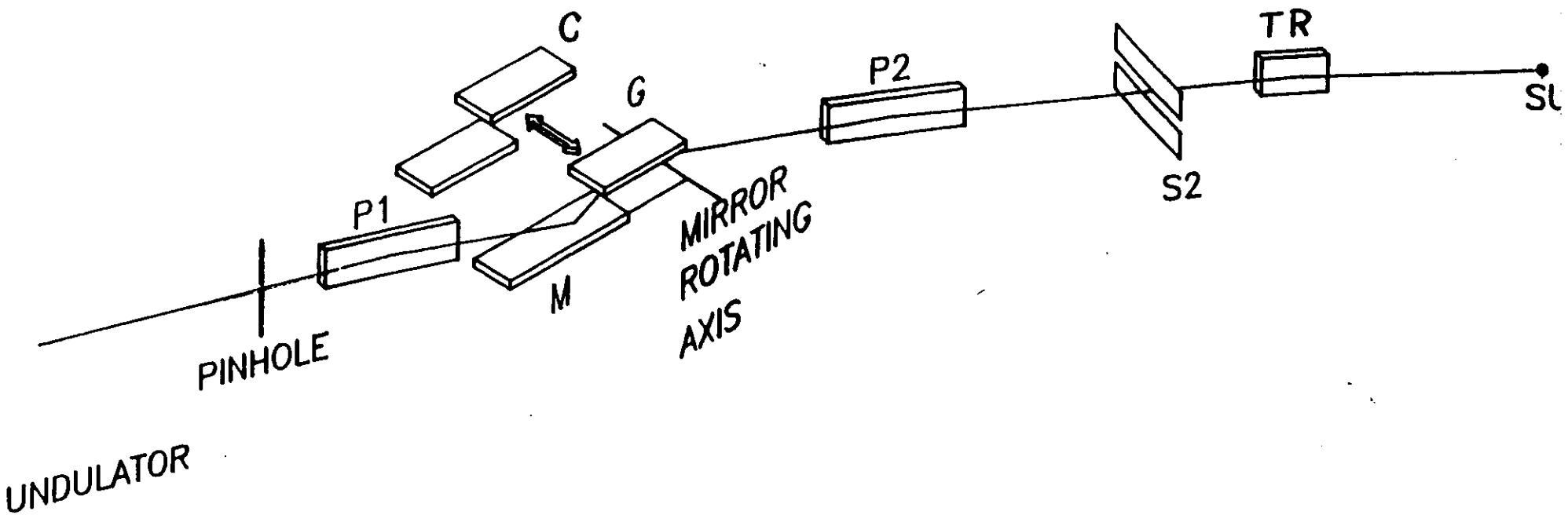

Modeling of Crystal Performance

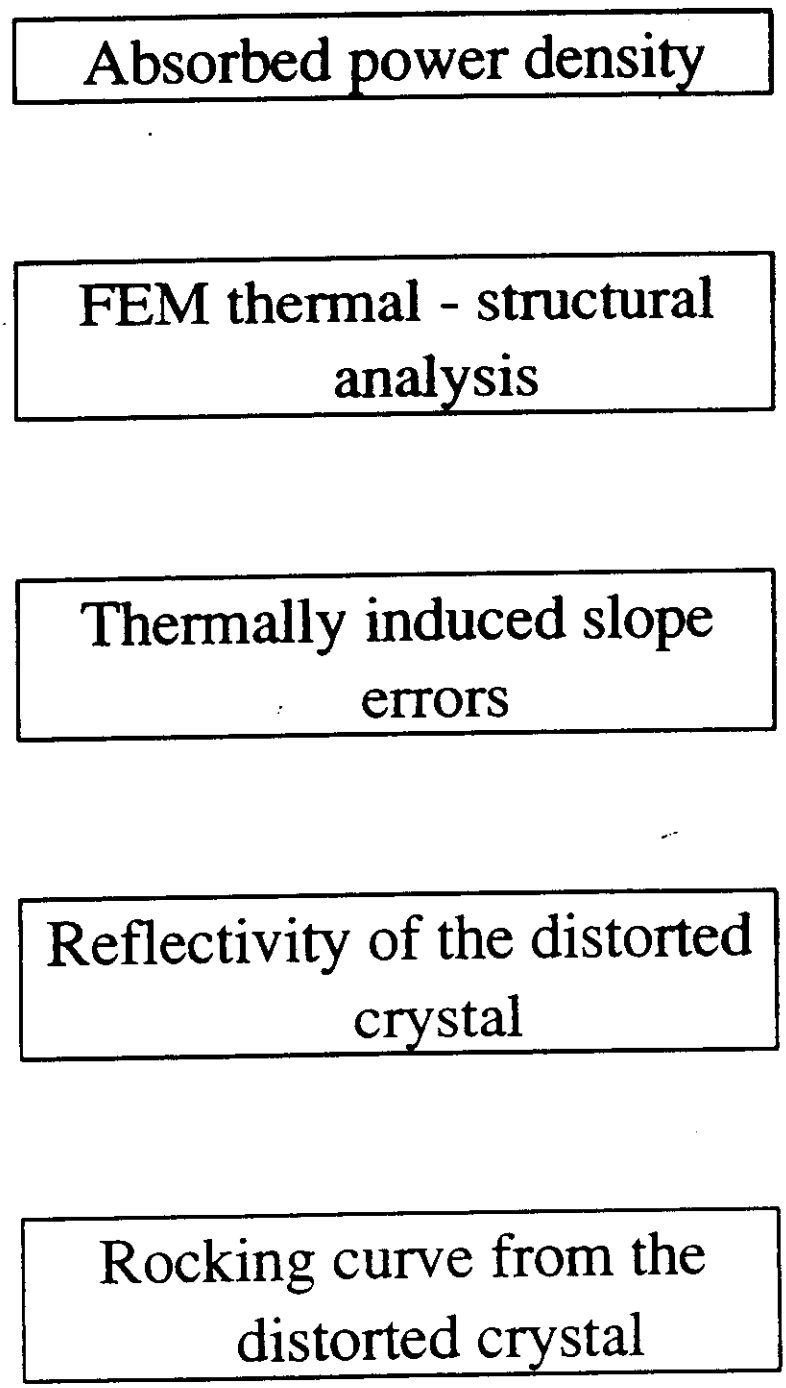

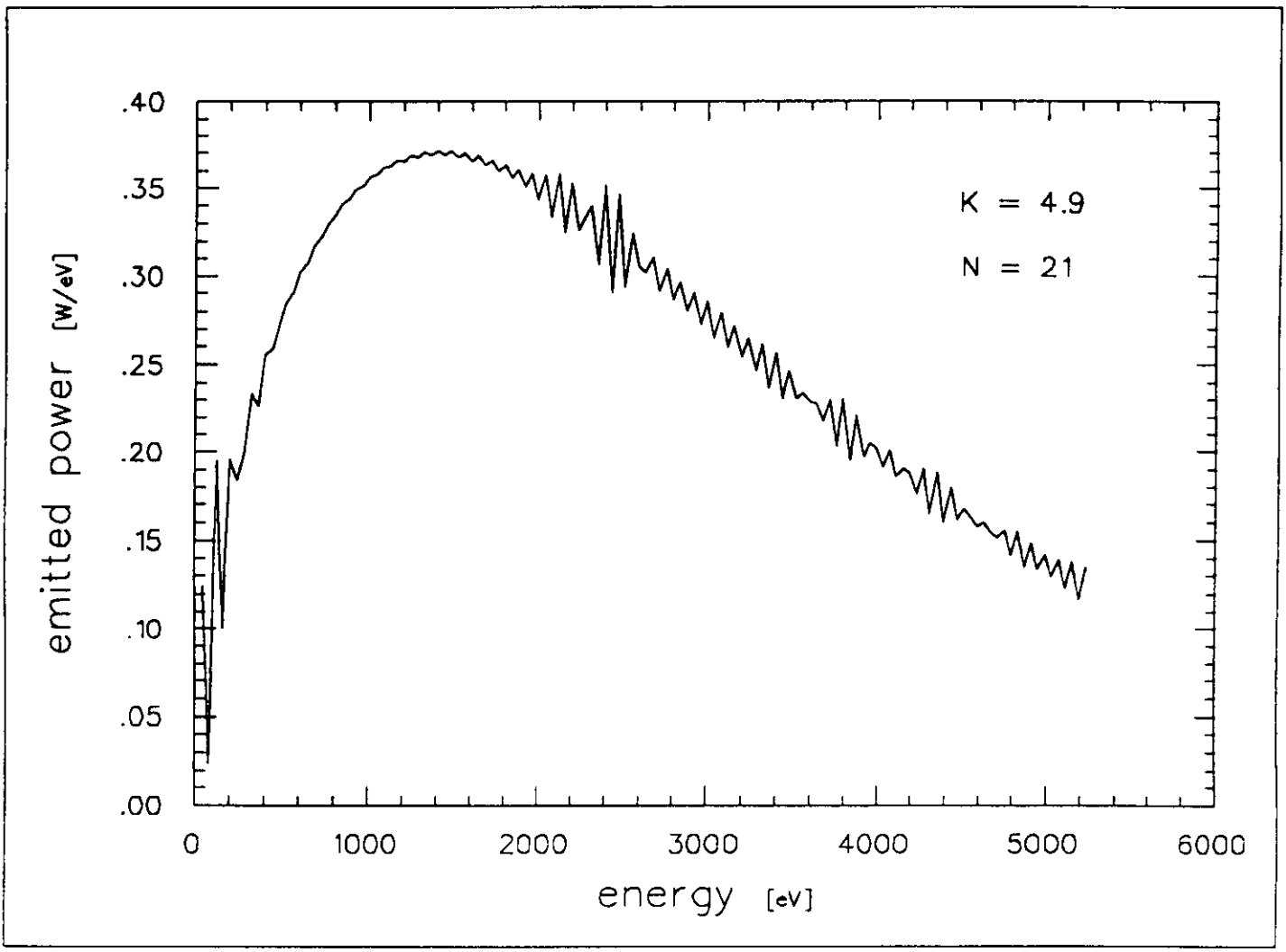
.40
.35
.30
.25
.20
.15
.10
.05
.00
emitted power [W/eV]
K = 4.9
N = 21
0
1000
2000
3000
4000
5000
6000
energy [eV]

ELETTRA parameters

Electron beam energy	1.5÷2.0	GeV
Maximum circulating current at 2.0 GeV	400	mA
Natural emittance ε	$7.1\ 10^{-9}$	π·m·rad
Beam size in the i.d.: Horizontal σ_x	240	μm
Beam size in the i.d.: Vertical σ_y	43	μm
Beam divergence in the i.d.: Hor. σ'_x	29.0	μrad
Beam divergence in the i.d.: Vert. σ'_y	16.5	μrad

ALOISA insertion device parameters

Period length	80	mm
Minimum gap (*)	20	mm
Number of periods per section	18	
Number of sections (**)	1	

(*) Operation modes of the insertion device:

. range 0.25 ÷ 2 keV in "undulator mode" i.e. tune using gap;

. up to 8 keV in "wiggler mode" i.e. set at minimum gap.

(**) In the future probably the number of section will increase up to three.

ALOISA layout parameters

Pinhole aperture: Horizontal σ_x'	$\pm$ 70	μrad
Pinhole aperture: Vertical σ_y'	$\pm$ 70	μrad
Exit slit – x-dimension	160	μm
Exit slit – y-dimension	20	μm
Demagnification of the P2	1/7	
Beam divergence on the sample: Hor. σ_x'	$\approx$ 500	μrad
Beam divergence on the sample: Vert. σ_y'	$\approx$ 500	μrad
Sample - detector distance	200	mm

Heat Loads on the First Crystal

Undulator period	80	mm
Deflection parameter K	6.5	
Number of periods N	**54**	
Electron beam energy	2.0	GeV
Current I	0.4	A
Horizontal Aperture σ_x'	**140**	μrad
Vertical Aperture σ_y'	**140**	μrad
Total emitted power in the cone P_t	**38**	W
x dimension (d = 21m)	2.94	mm
y dimension (d = 21m)	2.94	mm
Bragg angle at 3.0 keV (λ = 4.13 Å)	41.2	deg
x dimension on the crystal	**2.94**	mm
y dimension on the crystal	**4.46**	mm
Spot size (x/2·y/2·π)	10.30	mm^2
Power density on the crystal	**3.68**	W/mm^2
Bragg angle at 8.0 keV (λ = 1.55 Å)	14.3	deg
x dimension on the crystal	2.94	mm
y dimension on the crystal	11.90	mm
Spot size (x/2·y/2·π)	27.48	mm^2
Power density on the crystal	1.38	W/mm^2

Physical constant of the silicon

thermal conductivity of silicon	k_w	0.15	$W \cdot {}^oC^{-1} \cdot mm^{-1}$
elastic modulus of silicon	E	$1.58\ 10^5$	$N \cdot mm^{-2}$
Poisson ratio of silicon	ν	0.3	
thermal expansion coeff. of silicon	α	$2.5\ 10^{-6}$	${}^oC^{-1}$
thermal conductivity of copper	k_w	0.39	$W \cdot {}^oC^{-1} \cdot mm^{-1}$

Physical constant of the water

thermal conductivity	k_f	$6.0\ 10^{-4}$	$W \cdot {}^oC^{-1} \cdot mm^{-1}$
specific heat at constant pressure	c_p	4.180	$J \cdot {}^oC^{-1} \cdot g^{-1}$
specific heat per unit volume	ρ_c	$4.180\ 10^{-3}$	$J \cdot {}^oC^{-1} \cdot mm^{-3}$
dynamic viscosity	μ	$1\ 10^{-3}$	$g \cdot mm^{-1} \cdot sec^{-1}$

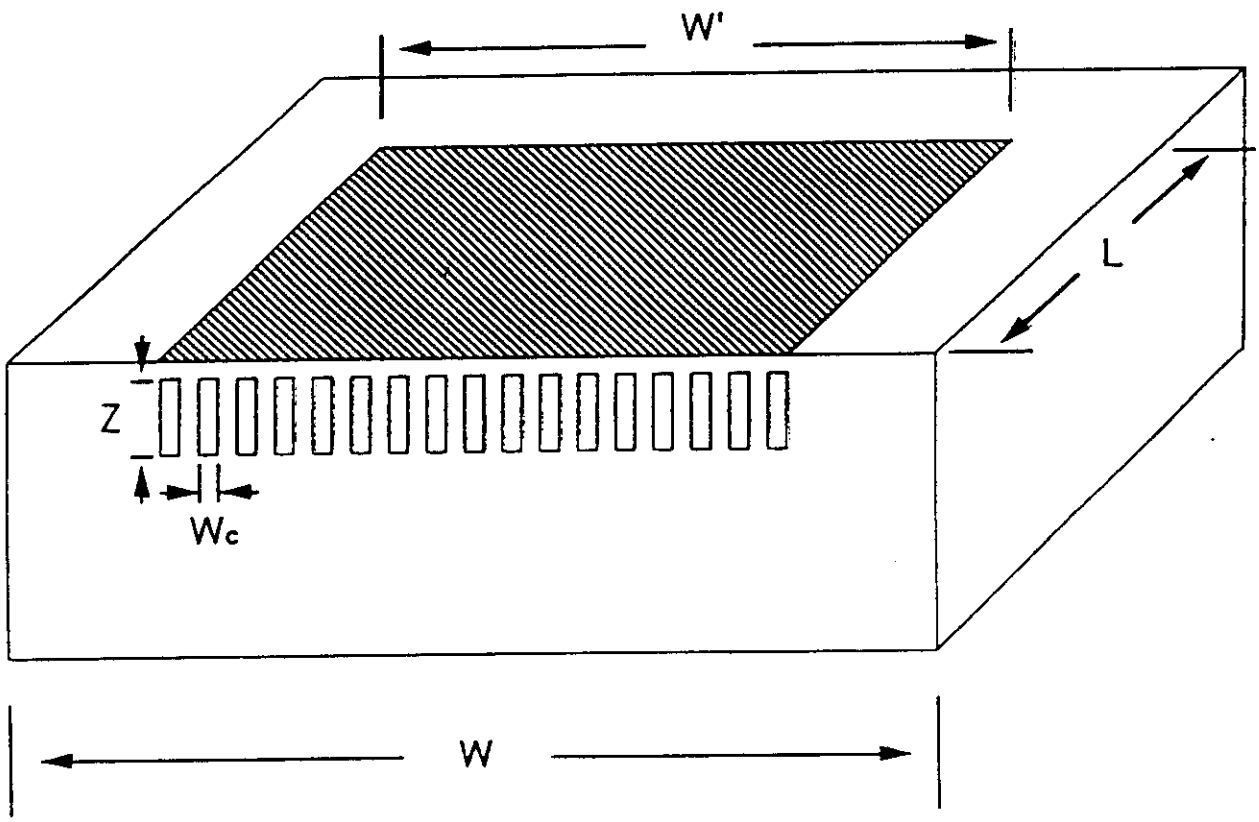
W'
L
Z
Wc
W

FEM analysis

- 3D model:
  thermal analysis DC3D20
  structural analysis C3D20

- Two-fold symmetry

- Two different water-cooling geometries:
  – Microchannels
  – Single channel inside the holder

- Heat load imposed by using the user subroutine DFLUX

- Film coefficient evaluted for each cooling system as a function of operative working conditions

- Kinematical conditions are applied only on the backside of the crystal, while the optical surface is left to expand freely.

References

[1] Nucl. Instr. Meth., Vol. A246 (1986).

[2] Rev. Sc. Instr. Vol. 60 (1989).

[3] Nucl. Instr. Meth., Vol. A291 (1990).

[4] ANL/APS/TM-6 (1990) (Argonne National Laboratory).

[5] Rev. Sc. Instr. Vol. 63 (1992).

[6] SPIE, Vol. 1739.

[7] Rev. Sc. Instr. Vol. 66 (1995).